

Redescription of *Phymolepis cuifengshanensis* (Antiarcha: Yunnanolepididae) using high-resolution computed tomography and new insights into anatomical details of the endocranium in antiarchs

Yajing Wang^{1, 2, 3}, Min Zhu^{Corresp. 1, 2, 3}

¹ Key Laboratory of Vertebrate Evolution and Human Origins of Chinese Academy of Sciences, Institute of Vertebrate Paleontology and Paleoanthropology, Beijing, China

² CAS Center for Excellence in Life and Paleoenvironment, Beijing, China

³ University of Chinese Academy of Sciences, Beijing, China

Corresponding Author: Min Zhu
Email address: zhumin@ivpp.ac.cn

Background. Yunnanolepidoids constitute either the basal-most consecutive segments or the most primitive clade of antiarchs, a highly diversified jawed vertebrate group from the Silurian and Early Devonian periods. Although the general morphology of yunnanolepidoids is well established, their endocranial features remain largely unclear, thus hindering our further understanding of antiarch evolution, and early gnathostome evolution. *Phymolepis cuifengshanensis*, a yunnanolepidoid from the Early Devonian of southwestern China, is re-described in detail to reveal the information on endocranial anatomy and additional morphological data of head and trunk shields.

Methods. We scanned the material of *P. cuifengshanensis* using high-resolution computed tomography and generated virtual restorations to show the internal morphology of its dermal shield. The dorsal aspect of endocranium in *P. cuifengshanensis* was therefore inferred. The phylogenetic analysis of antiarchs was conducted based on a revised and expanded dataset that incorporates ten new cranial characters.

Results. The lateroventral fossa of trunk shield and Chang's apparatus are three-dimensionally restored in *P. cuifengshanensis*. The canal that is positioned just anterior to the internal cavity of Chang's apparatus, probably corresponds to the rostrocaudal canal of euantiarchs. The endocranial morphology of *P. cuifengshanensis* corroborates a general pattern for yunnanolepidoids with additional characters distinguishing them from sinolepids and euantiarchs, such as a developed cranio-spinal process, an elongated endolymphatic duct, and a long occipital portion.

Discussion. In light of new data from *Phymolepis* and *Yunnanolepis*, we summarized the morphology on the visceral surface of head shield in antiarchs, and formulated additional ten characters for the phylogenetic analysis. These cranial characters exhibit a high degree of morphological disparity between major subgroups of antiarchs, and highlight the endocranial character evolution in antiarchs.

1 Author Cover Page

2

3

4 Article title:

5 Redescription of *Phymolepis cui Fengshanensis* (Antiarcha: Yunnanolepididae) using
6 high-resolution computed tomography and new insights into anatomical details of the
7 endocranium in antiarchs

8

9 Authors:

10 Yajing Wang^{1, 2, 3} and Min Zhu^{1, 2, 3}

11

12 Affiliations:

13 ¹Key Laboratory of Vertebrate Evolution and Human Origins of Chinese Academy of
14 Sciences, Institute of Vertebrate Paleontology and Paleoanthropology, Chinese
15 Academy of Sciences, Beijing 100044, China

16 ²CAS Center for Excellence in Life and Paleoenvironment, Beijing, 100044, China

17 ³University of Chinese Academy of Sciences, Beijing 100049, China

18

19 Corresponding author

20 Min Zhu, zhumin@ivpp.ac.cn

21 **ABSTRACT**

22 **Background.** Yunnanolepidoids constitute either the basal-most consecutive segments
23 or the most primitive clade of antiarchs, a highly diversified jawed vertebrate group from
24 the Silurian and Early Devonian periods. Although the general morphology of
25 yunnanolepidoids is well established, their endocranial features remain largely unclear,
26 thus hindering our further understanding of antiarch evolution, and early gnathostome
27 evolution. *Phymolepis cuifengshanensis*, a yunnanolepidoid from the Early Devonian of
28 southwestern China, is re-described in detail to reveal the information on endocranial
29 anatomy and additional morphological data of head and trunk shields.

30 **Methods.** We scanned the material of *P. cuifengshanensis* using high-resolution
31 computed tomography and generated virtual restorations to show the internal
32 morphology of its dermal shield. The dorsal aspect of endocranium in *P.*
33 *cuifengshanensis* was therefore inferred. The phylogenetic analysis of antiarchs was
34 conducted based on a revised and expanded dataset that incorporates ten new cranial
35 characters.

36 **Results.** The lateroventral fossa of trunk shield and Chang's apparatus are three-
37 dimensionally restored in *P. cuifengshanensis*. The canal that is positioned just anterior
38 to the internal cavity of Chang's apparatus, probably corresponds to the rostrocaudal
39 canal of euantiarchs. The endocranial morphology of *P. cuifengshanensis* corroborates a
40 general pattern for yunnanolepidoids with additional characters distinguishing them from
41 sinolepids and euantiarchs, such as a developed cranio-spinal process, an elongated
42 endolymphatic duct, and a long occipital portion.

43 **Discussion.** In light of new data from *Phymolepis* and *Yunnanolepis*, we summarized
44 the morphology on the visceral surface of head shield in antiarchs, and formulated
45 additional ten characters for the phylogenetic analysis. These cranial characters exhibit a
46 high degree of morphological disparity between major subgroups of antiarchs, and
47 highlight the endocranial character evolution in antiarchs.

48 **INTRODUCTION**

49 Antiarchs, one of the most diverse and widespread fish groups during the Middle
50 Paleozoic, have been resolved at the base of the diversification of jawed vertebrates in
51 most of recent phylogenetic studies (Brazeau, 2009; Davis, Finarelli & Coates, 2012;
52 Zhu et al., 2012; Giles, Rücklin & Donoghue, 2013; Zhu et al., 2013; Dupret et al., 2014;
53 Zhu, 2014; Giles, Friedman & Brazeau, 2015; Long et al., 2015; Qiao et al., 2016; Zhu et
54 al., 2016). It is noteworthy that King et al. (2016) corroborated the placoderm monophyly
55 and proposed antiarchs as a clade sister to petalichthyids and ptyctodonts based on the
56 Bayesian tip-dated clock methods. Since the first description of antiarchs in 1840
57 (Eichwald, 1840), their general morphology has been well established (Young & Zhang,
58 1992; Janvier, 1996; Young & Zhang, 1996; Zhu, 1996; Lukševičs, 2001; Young, 2008;
59 Young, 2010; Zhu et al., 2012; Long et al., 2015). However, the anatomical atlas of
60 endocranium in antiarchs is poorly known, largely due to the absence of perichondral
61 ossification (Denison, 1978). While the impressions on the overlying head shield help to
62 restore the endocranial morphology to some extent (Stensiö, 1948; Denison, 1978;
63 Moloshnikov, 2008), such as in Bothriolepididae (Stensiö, 1948; Young, 1984),
64 Asterolepididae (Obruchev, 1933; Stensiö, 1969), and *Minicrania lirouyji* (Zhu & Janvier,
65 1996), little attention has been paid to character transformations of antiarch endocrania
66 in lack of corresponding data from primitive antiarchs.

67 Yunnanolepidoids are endemic antiarchs discovered from the South China and
68 Indochina blocks (Liu, 1983; Pan & Dineley, 1988; Tông-Dzuy, Janvier & Phuong,
69 1996; Wang, Qu & Zhu, 2010). They are considered to be the most primitive antiarchs
70 because of the absence of characteristic dermal brachial process (Chang, 1978;
71 Zhang, 1978; Zhang, 1980; Young, 1981a; Long, 1983; Janvier, 1995; Zhu & Janvier,
72 1996; Carr, Johanson & Ritchie, 2009; Zhu et al., 2012), although their monophyly has
73 not yet reached a consensus (Janvier & Pan, 1982; Young & Zhang, 1996). To date,
74 yunnanolepidoids also represent the oldest known antiarchs, even though the date of
75 the oldest yunnanolepidoid *Shimenolepis* (Wang, 1991) has been revised to Late
76 Ludlow recently (Zhao et al., 2016).

77 Yunnanolepididae, a major clade of Yunnanolepidoidei, is characterized by the
78 small brachial fossa and the *crista transversalis interna posterior* lying in front of the
79 posterior process and pit of trunk shield. It includes the following seven genera:
80 *Yunnanolepis*, *Parayunnanolepis*, *Phymolepis*, *Mizia*, *Grammaspis*, *Chuanbeiolepis*
81 and *Yunlongolepis* (Chang, 1978; Zhang, 1978; Wang, 1988; Tông-Dzuy & Janvier,
82 1990; Zhu, 1996; Pan & Lu, 1997; Zhang, Wang & Wang, 2001; Pan et al., 2017).

83 *Phymolepis* Chang, 1978 (Figs. 1–3) is a yunnanolepid antiarch from the Lower
84 Devonian of South China. The first description of the type species of *Phymolepis*, *P.*
85 *cui Fengshanensis*, was based on material (IVPP V4425) from the Xitun Formation of
86 Cui Fengshan in Qujing, Yunnan (Chang, 1978; Zhang, 1978). Amongst all the referred
87 specimens of *P. cui Fengshanensis* (Chang, 1978), V4425.7 (Fig. 4), a trunk shield with a

88 row of medial marginal plates of pectoral fin, was later assigned to *Yunnanolepis parvus*
89 (Zhang, 1980: pl. 5, fig. 1). V4425.7 differs from the holotype and other referred
90 specimens of *P. cuifengshanensis* in its comparatively small size, a sharp median dorsal
91 ridge running throughout the anterior median dorsal plate, and the absence of a
92 conspicuous tergal angle of trunk shield. As such, we follow Zhang (1980) to remove
93 V4425.7 from *P. cuifengshanensis*.

94 Young and Zhang (1996) described three specimens from the Xitun Formation (IVPP
95 V9059.1–3) as *P. cuifengshanensis*, however these specimens are distinguishable
96 from V4425.2 (Fig.3), a referred specimen of *P. cuifengshanensis* preserving part of
97 the head shield (Chang, 1978). The orbital fenestra in V9059.1–3 is semilunar in
98 shape and occupies nearly half of the total breadth of the head shield. Accordingly, we
99 also remove V9059.1–3 from *P. cuifengshanensis*.

100 Zhu (1996) assigned additional material from the Xishancun Formation at
101 Liaokuoshan in Qujing (IVPP V10500.1–6, V10508.1–3) to *P. cuifengshanensis*, making
102 the first occurrence of this genus no later than early Lochkovian. He also revealed the
103 Chang's apparatus (Zhu, 1996: fig. 11A) and the lateroventral fossa of trunk shield
104 (Zhu, 1996: figs. 11F and 11G) in *P. cuifengshanensis*, and placed *Phymolepis* as the
105 sister taxon of *Mizia* in the phylogenetic analysis.

106 To have a deeper understanding of yunnanolepidoids, their cranial morphology in
107 particular, here we used high-resolution computed tomography (CT) to examine the
108 internal morphology of dermal shield in *P. cuifengshanensis*. On the basis of resulting
109 new data, *P. cuifengshanensis* was re-described in more detail. We also conducted the
110 phylogenetic analysis of antiarchs based on a new character matrix expanded and
111 revised from previous analyses (Zhu, 1996; Jia, Zhu & Zhao, 2010; Pan et al., 2017).
112 Several cranial characters were compared and discussed among subgroups of
113 antiarchs to illuminate the endocranial character transformations.

114

115 MATERIALS AND METHODS

116 Material

117 The specimens of *P. cuifengshanensis* in this study are housed at Institute of
118 Vertebrate Paleontology and Paleoanthropology (IVPP), Chinese Academy of
119 Sciences (CAS). The material was all collected from muddy limestone of the Xitun
120 Formation in Cuifengshan, Qujing, Yunnan Province.

121 The Xishancun, Xitun, Guijiatun and Xujiachong formations (in ascending
122 chronological order) represent the Early Devonian non-marine strata in Qujing District
123 (Liu & Wang, 1973; P'an et al., 1978; Zhu, Wang & Fan, 1994; Liu, Gai & Zhu, 2018).
124 The Xitun Formation consists mainly of grayish-green muddy limestone and mudstone
125 (Fang et al., 1985; Xue, 2012), yielding a rich biota (Cuifengshan Assemblage)
126 characterized by the diversification of sarcopterygians (Chang & Yu, 1981; Chang &

127 Yu, 1984; Zhu, Yu & Janvier, 1999; Zhu, Yu & Ahlberg, 2001; Zhu & Yu, 2002) and
128 primitive antiarchs including *Yunnanolepis*, *Parayunnanolepis*, *Zhanjilepis*,
129 *Chuchinolepis* and *Phymolepis*. Other fishes in the Xitun Formation include the
130 endemic agnathans (Liu et al., 2015), arthrodires (Dupret, Zhu & Wang, 2017),
131 actinopterygians (Zhu et al., 2006; Lu et al., 2016), acanthodians and chondrichthyans,
132 the latter two of which are mostly known from microvertebrate remains (Wang, 1984).
133 The Xitun Formation has been dated as late Lochkovian (c. 410 – 415million years
134 ago) with evidence from fossil assemblages (Gao, 1981; Fang et al., 1994; Zhao et al.,
135 2011; Xue, 2012).

136

137 **CT analysis**

138 V4425.2, which preserved the only head shield material for *Phymolepis* in addition to
139 the almost complete trunk shield, was CT scanned at the Key Laboratory of Vertebrate
140 Evolution and Human Origins of Chinese Academy of Science, Beijing, using the 225 KV
141 micro-tomography scanner (developed by Institute of High Energy Physics, CAS) with
142 following parameters: 150 kV voltage; 100 mA current; 32.93 μm voxel size. All scans
143 were conducted using a 720° rotation with a step size of 0.5° and an unfiltered aluminium
144 reflection target. A total of 1440 transmission images were reconstructed in a 2048 ×
145 2048 matrix of 1536 slices. The software Mimics v. 18.0 was applied for the three-
146 dimensional reconstruction (segmentation and rendering).

147

148 **Phylogenetic analyses**

149 The character matrix of antiarchs herein consists of 42 ingroup taxa, 2 outgroup
150 taxa (*Kujdanowiaspis* and *Romundina*), and 79 morphological characters. The matrix
151 is modified from those of Zhu (1996), Jia, Zhu & Zhao (2010) and Pan et al. (2017),
152 with revised codings and the addition of ten cranial characters. More details including
153 additional references and character re-formulations are provided in the Supplementary
154 Information.

155 We performed a traditional search in TNT v 1.5 (Goloboff et al., 2008), using 1000
156 random addition sequence replicates, saving 100 trees per replication. We assessed
157 nodal supports through bootstrap values with 100 pseudoreplicates and Bremer decay
158 indices. All characters were treated as equally weighted, and unordered (except
159 Characters 19, 49 and 50). Character state transformations to the nodes of one of the
160 most parsimonious trees (MPTs) were reconstructed in PAUP*4.0a (Swofford, 2003)
161 adopting DELTRAN and ACCTRAN optimizations respectively. Character mapping was
162 performed in MacClade 4.0 (Maddison & Maddison, 2000).

163

164

165 **RESULTS**

166 **Systematic paleontology**

167 Placodermi McCoy, 1848

168 Antiarcha Cope, 1885

169 Yunnanolepidoidei Gross, 1965

170 Yunnanolepididae Miles, 1968

171 *Phymolepis* Chang, 1978

172 **Type species.** *Phymolepis cui Fengshanensis* Chang, 1978

173 **Included species.** *Phymolepis guoruii* Zhu, 1996

174 **Emended diagnosis.** Yunnanolepididae in which the posterior median dorsal plate
175 bears a strong posterior process; the anterior median dorsal plate with anterior division
176 longer than posterior division; anterior ventral process and pit situated just below a
177 conspicuous tergal angle and at the same level of the lateral corners of the anterior
178 median dorsal plate; sharp median dorsal ridge between the tergal and posterior dorsal
179 angles.

180 **Remarks.** The diagnosis of this genus follows Zhu (1996) with a minor revision. While
181 examining V4425.2 based on high-resolution CT, we noticed that the anterior ventral
182 process and pit are situated at the level of the lateral corners of the anterior median
183 dorsal plate rather than behind it.

184

185 **PHYMOLEPIS CUIFENGSHANENSIS** Chang, 1978

186 (Figures 1–3, 5–11)

187

188 1978 *Phymolepis cui Fengshanensis* – Chang, p. 292, pl. XXV (5–7)

189 1978 *Phymolepis cui Fengshanensis* – Zhang, p. 147, figs. 10–12, pl. VI

190 1996 *Phymolepis cui Fengshanensis* – Zhu, p. 257, figs. 11–12, pls. I (8–10), IV (1–9)

191

192 **Holotype.** IVPP V4425.3, a relatively complete trunk shield (Figs. 1A–1C).

193 **Paratype.** IVPP V4425.6, a posterior median dorsal plate (Figs. 1D and 1E).

194 **Referred specimens.** IVPP V4425.1 (Fig. 2), trunk shield; V4425.2 (Fig. 3) nearly
195 complete dermal shield only missing the anteriormost portion of head shield and the
196 posterior median dorsal plate; V10500.1, left anterior dorsolateral plate; V10500.2,
197 V10508.1–3, posterior median dorsal plates; V10500.3, left posterior dorsolateral plate;
198 V10500.4, right posterior lateral plate; V10500.5, left anterior ventrolateral plate;
199 V10500.6, right posterior ventrolateral plate.

200 **Occurrence.** The material was collected from two sites (Cuifengshan and
201 Liaokuoshan) in Qujing city, eastern Yunnan, southwestern China.

202 **Emended diagnosis.** *Phymolepis* species in which the posterior process of the posterior
203 median dorsal plate reaches one third of the plate length; the median dorsal ridge of
204 trunk shield developed as a blunt elevation in front of the tergal angle and as a sharp
205 crest behind the tergal angle.

206 **Remarks.** The diagnosis follows Zhu (1996) with an addition of the shape of the median
207 dorsal ridge.

208

209 **Description**

210 **Reconstruction and ornamentation**

211 Using the complete specimen of *Yunnanolepis chii* (Zhang, 1978: V4423.101, fig. 1)
212 as a reference, *Phymolepis cuifengshanensis* could reach 84 mm in the dermal shield
213 length, and represents the largest known species among Yunnanolepididae.

214 This re-investigation of *P. cuifengshanensis* brings together all referred specimens
215 and leads to a new reconstruction (Figs. 5 and 6). The tentative restoration for the
216 missing pre-orbital portion of head shield follows that of *Y. chii* (Zhang, 1978: fig. 1).

217 Small, round tubercles are densely distributed on the dorsal surface of the head and
218 trunk shields. The tubercles are generally larger on various ridges and along outer
219 margins of head shield than elsewhere. They are aligned parallel to the sutures between
220 dermal plates, or radiated from the angles on the dorsal wall of trunk shield. In addition,
221 they tend to form the rows along the sensory grooves. The tubercles on the lateral wall of
222 the trunk shield are weakly developed and finer than those elsewhere. The ventral wall of
223 the trunk shield is sparsely covered with tubercles that are slightly larger than the rest of
224 the dermal shield.

225

226 **Head shield**

227 The orbital fenestra (orb, Figs. 7A and 7C) is comparatively small, and occupies about
228 one fourth of the breadth of the head shield (Table 1). The obstantic margin (om, Fig. 7B)
229 is straight and long, with the preobstantic corner of head shield (proc, Fig. 7A) at the
230 midway of the postorbital division. The posterior margin of the head shield between well-
231 marked postobstantic corners (ptoc, Figs. 7B and 7D), has convex lateral parts (formed
232 mainly by the posterior margin of the paranuchal plate) and a slightly embayed mesial
233 part (formed by the posterior margin of the nuchal plate). The obstructed nuchal area (nm,
234 Fig. 7A) occupies 27% length of the nuchal (Table 1).

235 The lateral plate (La, Fig. 7A) has long contact margins for surrounding dermal plates.
236 In visceral view, the anterior attachment area for the submarginal plate is missing,
237 however, the posterior attachment area on the lateral plate (a_1 , Figs. 7B and 7C)
238 continues onto the postmarginal plate (a_2 , Figs. 7B and 7C).

239 The postpineal plate (PP, Fig. 7A) is wider than long. Its anterior margin is concave,
240 unlike the straight margin in *Yunnanolepis*, *Mizia* and *Parayunnanolepis*. The postpineal
241 thickening (pp.th, Fig. 7A) is extremely developed as a prominent tuberculate elevation,
242 which totally encompasses the posterior border of the orbital fenestra and occupies
243 about half of the postpineal plate length. On the visceral surface, paired postorbital
244 cristae (cr.po, Fig. 7D) run somewhat obliquely along the anterior margin of the plate.
245 Two cristae on either side of the postpineal plate are separated far away by a faint
246 median ridge (mr, Fig. 7B), which lies at anterior margin of the plate and does not extend
247 backwards as in many euantiarchs.

248 The nuchal plate (Nu, Figs. 7A and 7B) is broadest across the anterolateral angle. The
249 postpineal notch is broad and deep. The posterolateral margin is about twice as long as
250 the anterolateral one (Table 1). The robust anterolateral ridge (alr, Fig. 7A) sits mainly in
251 the anterior division of the nuchal plate. The transverse nuchal crista (cr.tv, Fig. 7B) on
252 the visceral surface is well developed and thickened laterally.

253 The paranuchal plate (PNu, Figs. 7A and 7B) is as broad as it is long. The obtected
254 area of the plate is steeply inclined to the ornamented surface, especially near its suture
255 with the nuchal plate. The postmarginal plate (PM, Fig. 7A) is rhombic and longitudinally
256 extended. On the visceral surface, the attachment for the submarginal plate is narrower
257 posteriorly.

258

259 **Endocranium**

260 Like other antiarchs, only the dorsal aspect of the endocranium can be inferred in *P.*
261 *cuihengshanensis* from the impressions on the visceral surface of the head shield, which
262 is digitally visible with a high level of details.

263 The otico-occipital depression of *P. cuihengshanensis* is deeper posteriorly, along with
264 the gradually thickened paramarginal crista (cr. pm, Figs. 7B and 7D). This depression is
265 laterally extended at the suture between the lateral and paranuchal plates, where the
266 paramarginal crista lies underneath the infraorbital sensory groove. As such, the
267 paramarginal crista in *P. cuihengshanensis* with the convex median part, differs from the
268 straight one in asterolepidoids (Hemmings, 1978; Young, 1983) and laterally concave
269 one in bothriolepidoids (Chang, 1965; Young, 1988).

270 The anterolateral corner of the otico-occipital depression (p.apo, Figs. 7B and 7D),
271 which represents the imprint for the anterior postorbital process of endocranium (Young,
272 1984), is weakly developed and apically rounded. Significantly, it is located at the same
273 level with the posterior border of the orbital notch.

274 Near the posterior end of the paramarginal crista, the paranuchal plate is deeply
275 excavated by the large cavity (c.csp, Figs. 7B and 7D) for the cranio-spinal process of
276 the endocranium. The cavity is conical and tapers laterally with a B/L ratio of around 3.0;
277 its axis is perpendicular to the paramarginal crista (Figs. 8D–F).

278 The semicircular depressions (dsc, Figs. 7B and 7D) sit just in front of the level of
279 cranio-spinal processes. The anterior and posterior semicircular depressions are
280 relatively short, and meet in a confluence that is located midway between the posterior
281 border of the orbital notch and the transverse nuchal crista. As the lateral extension of
282 the otico-occipital depression roughly levels with the confluence, this lateral extension
283 appears to relate with the labyrinth cavity (d.sac?, Fig. 7D) as seen in *Arenipiscis westolli*
284 (Young, 1981b: fig. 6). In view of the otic region, which can be estimated by the position
285 of semicircular depressions, lies mainly in the anterior half of the otico-occipital
286 depression, so the occipital region of *P. cuifengshanensis* is fairly long compared with
287 euantiarchs.

288 Median to the posterior end of the semicircular depression, the internal pore for the
289 endolymphatic duct (d.end, Figs. 7B and 7D) is rounded and situated far ahead of the
290 transverse nuchal crista, while the external pore (d.end, Figs. 7A and 7C) is situated far
291 posteriorly at the anterior margin of the nuchal area. The distance between the
292 internal pores of both sides is 2.5 times longer than the distance between the external
293 ones. The digital visualization reveals that the endolymphatic duct of *P.*
294 *cuifengshanensis* is a long and roughly straight tube. It runs posterodorsally within the
295 nuchal plate, swings laterally while close to the midline of the plate and opens to the
296 exterior (Figs. 7A–C).

297 Posteriorly, a pair of supraoccipital pits (sop, Figs. 7B and 7D) is positioned just in front
298 of the transverse nuchal crista. This pit is easily distinguished from the internal pore of
299 the endolymphatic duct by its large size and ellipsoidal shape. The pit is dorsomedially
300 oriented within the nuchal plate, and gradually tapers off just beneath the ornamented
301 surface (Figs. 8A–C). The supraoccipital pit also occurs in *Vukhuclepis* (Racheboeuf et
302 al. 2006: fig. 4) and *Yunnanolepis* at the same position. It is noteworthy that Liu (1963: fig.
303 1) misidentified the supraoccipital pit in *Yunnanolepis* as the internal pore for the
304 endolymphatic duct.

305 Just anterior to the cavity for the cranio-spinal process, a corner (c.vg, Fig. 8F) in a
306 nearly right angle is set on approximately at the posterior end of a semicircular
307 depression level, and thus the hindmost level of the otic region. This corner is also
308 positioned between the anterior postorbital process and cranio-spinal process of
309 endocranium. Therefore, we tentatively interpret this corner as the depression of the
310 vagal process as it shares the same topological relationships to that of arthrodires and
311 petalichthyids.

312

313 **Trunk shield**

314 The trunk shield is fairly high, with a conspicuous tergal angle (Figs. 2C–2D; 9C–9D)
315 taking up almost half of the trunk shield height. The small pectoral fossa (pf, Fig. 1C) is
316 set just above the bottom of the trunk shield, and occupies a quarter of the lateral wall

317 height (Table 2). Both the dorsolateral and ventrolateral ridges of the trunk shield are
318 robust (dl, vl, Figs. 1C and 3D).

319 The dorsal wall has a convex anterior margin. The median dorsal, dorsal diagonal and
320 dorsal transverse ridges (dmr, ddr, dtr, Figs. 1–3A) on the dorsal wall radiate from the
321 tergal angle as in *Mizia longhuaensis*, *Yunnanolepis porifera* and *Chuchinolepis*
322 *qujingensis* (Zhu, 1996: figs. 4C, 5C–5D, 21A). The lateral wall carries the lateral and
323 oblique ridges (lr, or, Figs. 1C, 3D and 9D), which are widely developed in
324 yunnanolepidoids.

325 The main lateral line (lc, Figs. 2C, 3D and 10A) runs posteriorly very close and
326 subparallel to the dorsolateral ridge of trunk shield. It terminates at the end of the
327 dorsolateral ridge on the posterior dorsolateral plate.

328 The anterior median dorsal plate (AMD, Figs. 1–3A, 9A and 11A) is pentagonal in
329 shape. The posterolateral margin is embayed near its posterior end as in *Yunnanolepis*
330 (Zhang, 1980: fig. 3C). The concave posterior margin of the plate is delimited laterally by
331 distinct posterolateral angles (pla, Figs. 1A and 11A). The tergal angle lies at the same
332 level with the lateral corner of the plate. Internally, the anterior ventral pit (pt1, Fig. 11A)
333 with thin rim is located right beneath the tergal angle. It extends posteriorly to form a low
334 ridge (prv1, Fig. 11A).

335 The posterior median dorsal plate (PMD, Figs. 1D and 1E) bears a large posterior
336 process (pr.p, Fig. 1E), which occupies about two fifths of the plate in length and three
337 fourths in breadth. The dorsal median ridge and the posterior lateral ridges of both sides
338 (plr, Fig. 1D) converge to the posterior dorsal angle, which is developed as a small
339 nodule. The posterior corner of the plate (pa, Fig. 1D) is rounded. Internally, the *crista*
340 *transversalis interna posterior* (cr.tp, Fig. 1E) is developed as a low ridge just anterior to
341 the posterior ventral process (pt2, Fig. 1E).

342 The anterior dorsolateral plate (ADL, Figs. 2C, 3D, 9D) consists of articular, dorsal and
343 lateral laminae. The transversely extending articular fossa (f.ca, Fig. 2D and 9C) is
344 delimited by the supra- and infra-articular ridges (sar, iar, Fig. 2E). The supra-articular
345 ridge, which extends laterally from the postnuchal ornamented corner (pnoa, Figs. 2C,
346 3C and 9C), is longer than the infra-articular one. The dorsal lamina is slightly arched
347 with a dorsal diagonal ridge. The dorsal division of the ridge caused by Chang's
348 apparatus (r.C, Figs. 2E and 9D) is positioned on the lateral lamina adjacent to the
349 obstantic margin of the head shield.

350 The anterior ventrolateral plate (AVL, Figs. 9) consists of lateral and ventral laminae,
351 which meet at the ventrolateral ridge. The lateral lamina bears the ventral division of the
352 ridge caused by Chang's apparatus near its anterior margin. The ventral lamina shows a
353 shallow semilunar notch. Internally, both the posterior branchial lamina (pbl, Figs. 2D–E
354 and 10D) and *crista transversalis interna anterior* (cit, Figs. 2D–E and 10D) are strongly
355 developed. The posterior branchial lamina, ornamented by denticulate ridges, is present

356 close to the anterior margin of the trunk shield. It runs anteromedially from the lateral
357 lamina of the plate to the ventral lamina as a narrow band. The *crista transversalis*
358 *interna anterior* is located immediately behind the postbranchial lamina. Dorsally, the
359 crista extends from the AVL to the base of the articular fossa on the ADL (Figs. 2D, 2E
360 and 9C), where it is just behind Chang's apparatus (c.C, Fig. 10C). The left AVL overlaps
361 the right.

362 Between the posterior branchial lamina and *crista transversalis interna anterior*, a
363 canal (rc, Figs. 10A, D–F) is present just anterior to the internal cavity of Chang's
364 apparatus (Fig. 10B). The canal passes ventrally along the lateral wall of the trunk shield.
365 With a relatively large diameter, it probably carries both vessels and nerves and
366 corresponds to the rostrocaudal canal in *Chuchinolepis* (Young & Zhang, 1992),
367 sinolepids and euantiarchs, which is similarly positioned to supply the fin muscles
368 (Young, 2008).

369 The posterior dorsolateral plate (PDL, Fig. 9D) consists of the dorsal and lateral
370 laminae. The dorsal lamina is slightly less than twice as long as it is broad (Table 2).

371 The posterior lateral plate (PL, Figs. 2C, 3C and 9D) is arched along the lateral ridge
372 of trunk shield. The anteroventral margin is concave, and longer than the anterodorsal
373 one. The dorsal margin of the PL overlaps the PDL.

374 The posterior ventrolateral plate (PVL, Figs. 2C, 9B and 9D) consists of lateral and
375 ventral laminae. The subanal division of the ventral lamina is too short to define. The left
376 PVL overlaps the right one.

377 On the visceral surface of the trunk shield, a fossa (f.lv, Figs. 11B and 11C) is located
378 at the thickened junction of the AVL, PVL and PL plates, as in *Yunnanolepis* and
379 *Zhanjilepis* (Zhu, 1996). The fossa was termed the 'lateroventral fossa', and regarded as
380 a synapomorphy of yunnanolepids by Zhu (1996).

381 Posteriorly, a deeply grooved internal structure (cg, Fig. 11F) is developed along the
382 caudal opening of trunk shield. The groove has a smooth internal surface, delimited
383 anteriorly and posteriorly by the developed *crista transversalis interna posterior* and
384 posterior margins of trunk plates (PVL, PL and PDL) respectively. It consists of upper
385 and lower halves divided by a thin septum (ms, Figs. 11D and 11F). The similar structure
386 in *Yunnanolepis porifera*, as well as in *Pterichthyodes milleri* (Hemmings, 1978: fig. 15D),
387 was assumed to be related to internal fertilization (Long et al., 2015).

388 The semilunar plate (SL, Fig. 9B) is triangular in shape, and approximately twice as
389 broad as long. It is overlapped posteriorly by the AVL. Internally, the postbranchial
390 lamina extends anteromesially from the AVL onto the semilunar plate, and meets the
391 lamina from the opposite.

392 The median ventral plate (MV, Figs. 1B, 2B and 9B) is rhombic. The exposed surface
393 accounts for two fifths of the ventral wall of trunk shield in length and a half of the ventral
394 wall in breadth. The plate is thinner than the surrounding plates.

395

396 **DISCUSSION**397 **Anatomical comparisons of several cranial characters in antiarchs**

398 The restoration of the endocranium in antiarchs was mainly based on the imprints of
399 its dorsal aspect on the visceral surface of the head shield (Stensiö, 1948; Stensiö, 1969;
400 Miles, 1971; Denison, 1978; Young, 1984). The exception was *Minicrania*, which
401 preserved the internal cast of the endocranial canals and part of the cranial cavity, thus
402 providing information on its deeper endocranial structures (Zhu & Janvier, 1996).

403 In yunnanolepidoids, the visceral surface of head shield was known in *Yunnanolepis*
404 (Liu, 1963: fig. 1) and *Chuchinolepis* (Tông-Dzuy & Janvier, 1990: fig. 17). The digital
405 visualization of *Phymolepis* shows not only its visceral surface of head shield but also
406 some internal architecture within the dermal plates, such as the trajectory of the
407 endolymphatic duct and the cavity for the cranio-spinal process. We also re-examine
408 the holotype (V2690.1, Fig. 12A) and one referred specimen (V4423.3, Fig. 12B) of *Y.*
409 *chii* from the Early Devonian of Qujing, and provide more details for the visceral
410 surface of head shield in *Yunnanolepis*. Based on these new data, we make
411 comparisons in antiarchs, and show a high degree of morphological disparity with
412 respect to the endocranium.

413 **Anterior postorbital process.** The endocrania of gnathostomes share a developed
414 lateral projection where the orbits meet the otic capsules (Brazeau & Friedman, 2014).
415 This process was termed the ‘anterior postorbital process’ in placoderms, and deemed
416 as supporting the hyoid arch articulation and delimiting the posterior boundary of the
417 spiracular chamber by its anterior surface (Young & Zhang, 1996; Brazeau &
418 Friedman, 2014). The positional differences of the anterior postorbital process (and
419 associated cranial nerves) along the longitudinal axis of dermal shield were thought to
420 be informative for phylogenetic analysis (Carr et al., 2009; Dupret et al., 2017).

421 Antiarchs have a well-developed anterior postorbital process. The process
422 extending in front of the anterior border of the orbital notch, has been considered as
423 one of the synapomorphies uniting *Bothriolepis* and *Grossilepis* (Zhang & Young,
424 1992; Zhu, 1996; Jia, Zhu & Zhao, 2010; Pan et al., 2017). Accordingly, the process
425 behind the anterior border of the orbital notch is referred to a plesiomorphy of
426 antiarchs and this state has been simply summarized as “anterior postorbital process
427 short” in previous phylogenetic analyses (Zhang & Young, 1992).

428 When examining the short anterior postorbital process in antiarchs, we recognized
429 that this state can be subdivided into two conditions: the anterior postorbital process at
430 the same level with the posterior border of the orbital notch in yunnanolepidoids,
431 *Minicrania* (Zhu & Janvier, 1996), and probably *Sinolepis* (Liu & P'an, 1958; Long, 1983);
432 the process anteriorly beyond the posterior border of the orbital notch, but behind its
433 anterior border in euantiarchs excluding *Grossilepis* and *Bothriolepis*. In this case, the

434 distinction between these two conditions can be added to the transformation series of the
435 anterior postorbital process.

436 **Postorbital crista.** The postorbital crista in antiarchs separates the otico-occipital
437 depression from the orbital region in front. In several euantiarchs, the crista extends
438 obliquely from the crest of the spiracular groove on the lateral plate to the nuchal plate
439 as a mesial wall of the semicircular depression, such as in *Bothriolepis* (Stensiö, 1948),
440 *Monarolepis* (Young & Gorter, 1981), *Pterichthyodes* (Hemmings, 1978) and
441 *Wufengshania* (Pan et al., 2017). For the rest of antiarchs including yunnanolepidoids,
442 the postorbital crista runs from the lateral plate to the postpineal plate rather than the
443 nuchal plate as a transversely directed crest embracing the suborbital fenestra
444 posteriorly.

445 **Supraotic thickening.** The supraotic thickening (Young, 1983: sot, fig. 3D) is
446 bounded posteriorly by the transverse nuchal crista and extensively developed at its
447 connection with the crista. As the supraotic thickening is porous, different from the rest
448 of dermal skeleton in microstructure, it was considered as a junction that is co-ossified
449 with both the endocranium and overlying head shield (Stensiö, 1948; Karatajūte-
450 Talimaa, 1963; Moloshnikov, 2004; Moloshnikov, 2008). Euantiarchs have a persistent
451 supraotic thickening with the exception of *Microbrachius*, which bears a deep groove
452 throughout the whole length of the otico-occipital depression (Hemmings, 1978: figs.
453 25C–F). The presence of this thickening on the visceral surface of euantiarchs is in
454 stark contrast to the condition in yunnanolepidoids, *Minicrania* and sinolepids, which
455 lack any thickening in the corresponding area.

456 **Median occipital crista.** This crista was first identified and named by Stensiö (1931:
457 cro, figs. 11 and 12) in *Bothriolepis*, and was also termed the ‘posterior median process’
458 by Hemmings (1978) in *Pterichthyodes*. Lying on the descending lamina of occipital part
459 of the head shield, it is separated from the otico-occipital depression by the transverse
460 nuchal crista in euantiarchs. A shallow depression of levator muscles (termed the
461 ‘insertion fossa on head shield for levator muscles’) usually flanks on each side of the
462 crista. In sinolepids, such as *Grenfellaspis* (Ritchie et al., 1992), the insertion fossa is
463 elongated as that in euantiarchs but lacks the median crista. In yunnanolepidoids, the
464 insertion fossa is either very short (*Yunnanolepis*, Fig. 12B), or totally absent
465 (*Phymolepis*, Fig. 7B).

466 **Posterior process of head shield.** The posterior process of head shield (prnm, see
467 Young (1988): figs. 7B, 37C and 44A) in euantiarchs, also termed the ‘nuchal process’
468 or ‘posterior median process’ (Long & Werdelin, 1986; Moloshnikov, 2004;
469 Moloshnikov, 2008; Moloshnikov, 2010), was first identified and named by Stensiö
470 (1931: figs. 4, 9 and 12). Although the median occipital crista is usually continuous with
471 the posterior process of head shield, the process is apparently independent of the crista
472 in development as evidenced by *Asterolepis* and *Remigolepis*, which possess the
473 process but lack the crista. The process is usually developed in euantiarchs, in contrast

474 to its absence in yunnanolepidoids and sinolepids.

475 Among non-antiarch placoderms, the posterior process is also known in
476 petalichthyids (Liu, 1991; Pan et al., 2015) and arthrodires (Wang & Wang, 1983;
477 Gardiner & Miles, 1990; Young, 2005; Carr & Hlavin, 2010; Rücklin, Long & Trinajstić,
478 2015).

479 **The cavity for cranio-spinal process.** The cranio-spinal process was named by
480 Nielsen (1942), and also termed the 'supravagal process' by Stensiö (1969) and the
481 'paroccipital process' by Eaton (1939). It is widely developed in early gnathostomes,
482 including arthrodires (Young, 1979), petalichthyids (Stensiö, 1925), acanthodians
483 (Miles, 1973), actinopterygians (Patterson, 1975) and dipnoans (Miles, 1977).
484 However, the cavity for cranio-spinal process on the visceral surface of head shield,
485 which might function for fixing the endocranium to the external bony shield, is only found
486 in primitive antiarchs and some arthrodires.

487 The cranio-spinal process in yunnanolepidoids is strongly developed, as indicated
488 by the large cavity for the process. The process and the corresponding cavity in
489 euantiarchs were either reduced or absent (Young, 1984).

490 **Supraoccipital pit.** The supraoccipital pit of the head shield is present for housing the
491 endocranial supraoccipital process. It is bounded posteriorly by the transverse nuchal
492 crista in yunnanolepidoids. The same condition is also seen in *Grenfellaspis* (Ritchie
493 et al., 1992) and *Minicrania*, despite the supraoccipital pit in the latter has ever been
494 interpreted as impression of endolymphatic sac (Zhu & Janvier, 1996; Dupret et al.,
495 2017). In euantiarchs, the supraoccipital pit is only seen in few *Bothriolepis* species
496 with two different positions: either immediately anterior to the transverse nuchal crista
497 as exemplified by *B. tatongensis* (Long & Werdelin, 1986), or on the transverse nuchal
498 crista as in *B. macphersoni* and *B. portalensis* (Young, 1988).

499 In non-antiarch placoderms, the supraoccipital pit has been observed in
500 petalichthyids (Liu, 1991: cv.ifNu, fig. 2), and most arthrodires, including
501 Holonematidae (Miles, 1971: tf; figs. 53 and 117; Young, 2005: if.pt, fig. 2C),
502 Buchanosteidae (Young, 1981b: if.pt, fig. 6), Coccosteioidea (Miles & Westoll, 1968:
503 p.pts.Nu, fig. 2a), Dunkleosteioidea (Zhu, Zhu & Wang, 2016: f.pt.u, fig. 5; Carr &
504 Hlavin, 2010: pt.u, fig. 6A) and Dinichthyidae (Carr & Hlavin, 2010: pt.u, fig. 1A).

505 **Trajectory of endolymphatic duct.** The trajectory of the endolymphatic duct through
506 the dermal bone in respect of length and orientation mainly depends on the relative
507 position between the internal and external pores. This character was considered
508 informative for the resolution of placoderm interrelationships. The trajectory had ever
509 been decomposed into two states: vertical (a trait in most non-arthrodire placoderms),
510 long and oblique (a trait shared by arthrodires) by Goujet & Young (1995). Coates &
511 Sequeira (1998) considered the posteriorly oriented duct as a primitive character of
512 gnathostomes as it is shared by agnathans, placoderms and osteichthyans. Brazeau

513 (2009) suggested the presence of posterodorsally angled trajectory as an arthrodire
514 character and the absence of oblique trajectory of endolymphatic duct as a character
515 shared by antiarchs, *Brindabellaspis* and petalichthyids. Our study herein shows the
516 condition in antiarchs is more complicated than previously thought.

517 In antiarchs, the distance between the internal pores is usually greater than that of
518 external ones (Stensiö, 1948; Karatajūte-Talimaa, 1966; Long, 1983), and the
519 endolymphatic duct extends dorsomesially. As the external pore of endolymphatic duct
520 is always positioned close to the posterior edge of the nuchal plate in antiarchs, the
521 relative position of the internal pore along the antero-posterior axis reflects the relative
522 length and orientation of the endolymphatic duct.

523 In yunnanolepidoids, the internal pore of endolymphatic duct is located far in front of
524 the transverse nuchal crista, and thus far from the external pore. As such, the
525 endolymphatic duct is elongated through the nuchal plate and obliquely oriented.
526 Sinolepids (Ritchie et al., 1992; Janvier, 1996) and euantiarchs differ in having a short,
527 slight oblique endolymphatic duct as the internal pore is positioned just anterior to the
528 external one.

529 In non-antiarch placoderms, the elongated endolymphatic duct is also present in
530 arthrodires (Young, 2010; Dupret et al., 2017). However, the endolymphatic duct of
531 arthrodires is directed dorsolaterally, not dorsomesially as in antiarchs.

532 **Occipital portion of endocranium.** The internal pore for the endolymphatic duct in
533 antiarchs, is located roughly at the posterior boundary of the semicircular depression on
534 the visceral surface of head shield as that in arthrodires (Zhu, Zhu & Wang, 2016), hence
535 we use this pore as a proxy to denote the otic-occipital boundary. Taking the length of
536 the otic-occipital depression as the constant variable in antiarchs, the length between the
537 internal pore of endolymphatic duct and the posterior border of otic-occipital depression
538 represents the occipital proportion in endocranium.

539 In yunnanolepidoids, the internal pore on the visceral surface of the head shield is far
540 from the transverse nuchal crista as described above, implying the occipital portion of the
541 endocranium is elongated as in arthrodires (Zhu, Zhu & Wang, 2016). By comparison,
542 the occipital portion is short in other antiarchs (Stensiö, 1948; Ritchie et al., 1992).

543 **Confluence of anterior and posterior semicircular canals.** The anterior and
544 posterior semicircular canals meet at the confluence in the medial part of the inner ear
545 (Dupret et al., 2017a). As the posterior border of orbital notch and the transverse nuchal
546 crista roughly border the anterior and posterior margins of the otic-occipital depression
547 respectively, we can use them as references to estimate the relative position of the
548 confluence in endocranium.

549 In yunnanolepids and *Minicrania* (Zhu, 1996), the confluence is halfway between
550 the posterior border of the orbital notch and the transverse nuchal crista. By
551 comparison, the confluence is closer to the transverse nuchal crista than to the

552 posterior border of orbital notch in sinolepids and euantiarchs.

553

554 **Phylogenetic results**

555 The maximum parsimony analysis yields 726 MPTs of 179 steps each (consistency
556 index= 0.4693; retention index= 0.8045). All the MPTs are summarized as a strict
557 consensus tree (Fig. 13A) and a 50% majority-rule consensus tree (Fig. 13B). One MPT
558 is selected to illustrate the character transformations at nodes (Fig. 14A), and the list of
559 synapomorphies defining various nodes is shown in Supplementary Information.

560 Antiarchs (Fig. 14A: node 1) are characterized by up to 10 synapomorphies including
561 two newly proposed cranial features (Character 27⁰, absence of posterior process of
562 head shield; Character 38¹, presence of supraoccipital pit). Character 27 shows a
563 reversal in euantiarchs (Fig. 14A: node 15). Character 38 is a highly homoplastic
564 character, and shows a reversal in euantiarchs and a parallelism in *Bothriolepis*.

565 Yunnanolepidoids (Fig. 14A: node 2) form the basal members of antiarchs, consistent
566 with the position as they were first phylogenetically analysed (Zhu, 1996). However in
567 new scenario, *Chuchinolepis*, *Vanchienolepis* and a clade formed by yunnanolepids,
568 *Zhanjilepis* and *Heteroyunnanolepis* fall into a polytomy with remaining antiarchs. In
569 yunnanolepids, *Yunnanolepis* is the sister group of a polytomic clade comprising
570 *Phymolepis*, *Mizia* and *Parayunnanolepis*.

571 Four new cranial characters provide further support the monophyly of euantiarchs (Fig.
572 14A: node 15), including one uniquely shared character (Character 36¹, anterior
573 postorbital process lying in front of posterior level of orbital notch) and three homoplastic
574 characters (Character 26¹, presence of median occipital pit of head shield; Character 27¹,
575 presence of posterior process of head shield and Character 38⁰, absence of
576 supraoccipital pit of head shield).

577 Microbrachiids (Fig. 14A: node 16) are resolved as the sister group of the remaining
578 euantiarchs, and the conventional bothriolepidoids are resolved as a paraphyletic
579 assemblage. These results are congruent with previous analyses of Zhu (1996) and Pan
580 et al. (2017). Relationships of the remaining bothriolepidoids (Fig. 14A: node 19) are
581 completely unresolved in the strict consensus tree, which may be related to the large
582 number of missing data in some of them. Euantiarchs excluding microbrachiids bear one
583 uniquely shared endocranial character (Character 25¹, presence of supraotic thickening
584 of head shield).

585 Our analysis that incorporate new cranial characters yields resultant trees, which are
586 consistent with previous resolutions of Zhu (1996), Jia, Zhu & Zhao (2010) and Pan et al.
587 (2017) in broad phylogenetic pattern. Under the new phylogenetic scenario, we can trace
588 the character transformations relating to the dorsal aspect of endocranium in antiarchs.

589 Yunnanolepidoids (Figs. 7, 12 and 14A) and *Minicrania* show primitive character states,

590 such as the anterior postorbital process being posteriorly positioned (Character 36⁰),
591 presence of cranio-spinal process (Character 37¹) and supraoccipital process (Character
592 38¹), anterior and posterior semicircular canals being anteriorly positioned (Character
593 39⁰), long endolymphatic duct (Character 40⁰), and long occipital portion (Character 41⁰).

594 At the node comprising sinolepids and euantiarchs (Fig. 14A: node 10), there are two
595 derived endocranial character states: short endolymphatic duct (Character 40¹) and
596 short occipital region (Character 41¹). Euantiarchs differ from sinolepids in possessing
597 the following derived states: the anterior postorbital process lying in front of the posterior
598 level of orbital notch (Character 36¹), and the absence of the supraoccipital process
599 (Character 38⁰). In short, there exists a large morphological disparity relating to the
600 dorsal aspect of endocranium between yunnanolepidoids, sinolepids and euantiarchs.

601

602 CONCLUSIONS

603 The re-investigation of *Phymolepis cuifengshanensis* with assistance of high-
604 resolution CT scanning, offers comprehensive information for this taxon and new insights
605 into the morphology and phylogeny of antiarchs.

606 The exoskeleton of *Phymolepis cuifengshanensis* shows typical yunnanolepid
607 characters, such as the small orbital fenestra, presence of both developed postbranchial
608 lamina and *crista transversalis interna anterior* on the trunk shield. The endocranium of *P.*
609 *cuifengshanensis* also resembles that of other yunnanolepidoids in the presence of
610 developed cranio-spinal process and supraoccipital process, the anterior postorbital
611 process lying at the same level with the posterior border of the orbital notch, elongated
612 endolymphatic duct and long occipital region.

613 We compare cranial characters among subgroups of antiarchs, and formulate ten
614 additional characters that deemed to be of phylogenetic significance. Phylogenetic
615 analysis of a revised and expanded dataset draws new perspectives on the
616 interrelationships of antiarchs, and corroborates the monophyly of yunnanolepidoids by
617 the presence of cavity for cranio-spinal process.

618 The character transformations relating to the dorsal aspect of endocranium in
619 antiarchs are inferred under the new phylogenetic scenario. By comparison to
620 yunnanolepidoids and *Minicrania*, which retain several primitive endocranial traits,
621 sinolepids and euantiarchs evolved two apomorphic features (short endolymphatic duct
622 and short occipital portion). Euantiarchs are more derived in the anterior postorbital
623 process lying in front of the posterior level of orbital notch, and the absence of the
624 supraoccipital process.

625

626 ACKNOWLEDGMENTS

627 We thank Dinghua Yang for life restoration, Xiaocong Guo for suggestions on the

628 interpretative drawings, You-an Zhu for discussions on arthrodire characters, Liantao Jia
629 and Wei Gao for the assistance to take photographs.

630

631 REFERENCES

632 Brazeau MD. 2009. The braincase and jaws of a Devonian 'acanthodian' and modern
633 gnathostome origins. *Nature* 457:305-308. DOI: 10.1038/nature07436.

634 Brazeau MD, Friedman M. 2014. The characters of Palaeozoic jawed vertebrates.
635 *Zoological Journal of the Linnean Society* 170:779-821. DOI: 10.1111/zoj.12111.

636 Carr RK, Hlavin WJ. 2010. Two new species of *Dunkleosteus* Lehman, 1956, from the
637 Ohio Shale Formation (USA, Famennian) and the Kettle Point Formation (Canada,
638 Upper Devonian), and a cladistic analysis of the Eubrachythoraci (Placodermi,
639 Arthrodira). *Zoological Journal of the Linnean Society* 159:195-222. DOI:
640 10.1111/j.1096-3642.2009.00578.x.

641 Carr RK, Johanson Z, Ritchie A. 2009. The phyllolepid placoderm *Cowralepis*
642 *mclachlani*: Insights into the evolution of feeding mechanisms in jawed vertebrates.
643 *Journal of Morphology* 270:775-804. DOI: 10.1002/jmor.10719.

644 Chang K-J. 1965. New antiarchs from the Middle Devonian of Yunnan. *Vertebrata*
645 *PalAsiatica* 9:1-9.

646 Chang K-J. 1978. Early Devonian antiarchs from Cuifengshan, Yunnan. In: Institute of
647 Geology and Mineral Resources of the Chinese Academy of Geological Sciences,
648 ed. *Symposium on the Devonian System of South China*. Beijing: Geological Press,
649 292-297.

650 Chang M-M, Yu X-B. 1981. A new crossopterygian, *Youngolepis praecursor*, gen. et sp.
651 nov., from Lower Devonian of E. Yunnan, China. *Scientia Sinica* 24:89-99.

652 Chang M-M, Yu X-B. 1984. Structure and phylogenetic significance of *Diabolichthys*
653 *speratus* gen. et sp. nov., a new dipnoan-like form from the Lower Devonian of
654 eastern Yunnan, China. *Proceedings of the Linnean Society of New South Wales*
655 107:171-184.

656 Coates MI, Sequeira SEK. 1998. The braincase of a primitive shark. *Transactions of the*
657 *Royal Society of Edinburgh: Earth Sciences* 89:63-85.

658 Cope ED. 1885. The position of *Pterichthys* in the system. *American Naturalist* 19:289-
659 291.

660 Davis SP, Finarelli JA, Coates MI. 2012. *Acanthodes* and shark-like conditions in the last
661 common ancestor of modern gnathostomes. *Nature* 486:247-250. DOI:
662 10.1038/nature11080.

663 Denison RH. 1978. Placodermi. In: Schultze HP, ed. *Handbook of Paleichthyology*, vol
664 2. Stuttgart: Gustav Fischer Verlag, 128.

665 Dupret V, Sanchez S, Goujet D, Ahlberg PE. 2017. The internal cranial anatomy of
666 *Romundina stellina* Orvig, 1975 (Vertebrata, Placodermi, Acanthothoraci) and the
667 origin of jawed vertebrates-Anatomical atlas of a primitive gnathostome. *PLoS One*

- 668 12:e0171241. DOI: 10.1371/journal.pone.0171241.
- 669 Dupret V, Sanchez S, Goujet D, Tafforeau P, Ahlberg PE. 2014. A primitive placoderm
670 sheds light on the origin of the jawed vertebrate face. *Nature* 507:500-503. DOI:
671 10.1038/nature12980.
- 672 Dupret V, Zhu M, Wang J-Q. 2017. Redescription of *Szelepis* Liu, 1981 (Placodermi,
673 Arthrodira), from the Lower Devonian of China. *Journal of Vertebrate Paleontology*
674 37:e1312422. DOI: 10.1080/02724634.2017.1312422
- 675 Eaton TH. 1939. A paleoniscid braincase. *Journal of the Washington Academy of*
676 *Sciences* 29:441-451.
- 677 Eichwald Elv. 1840. Geognostische ersicht von Esthland und den Nachbar-Gegenden.
678 *Neues Jahrbuch der Mineralogie, Geologie und Paläontologie* 1840:421-430.
- 679 Fang R-S, Jiang N-R, Fan J-C, Cao R-G, Li D-Y, 1985. *The Middle Silurian and Early*
680 *Devonian Stratigraphy and Palaeontology in Qujing District, Yunnan*. Kunming:
681 Yunnan People's Publishing House.
- 682 Fang Z-J, Cai C-Y, Wang Y, Li X-X, Wang C-Y, Geng L-Y, Wang S-Q, Gao L-D, Wang
683 N-Z, Li D-Y. 1994. New advance in the study of the Silurian-Devonian Boundary in
684 Qujing, East Yunnan. *Journal of Stratigraphy* 18:81-90.
- 685 Gao L-D. 1981. Devonian spore assemblages of China. *Review of Palaeobotany and*
686 *Palynology* 34:11-23.
- 687 Gardiner BG, Miles RS. 1990. A new genus of eubrachythoracid arthrodire from Gogo,
688 Western Australia. *Zoological Journal of the Linnean Society* 99:159-204.
- 689 Giles S, Friedman M, Brazeau MD. 2015. Osteichthyan-like cranial conditions in an Early
690 Devonian stem gnathostome. *Nature* 520:82-85. DOI: 10.1038/nature14065.
- 691 Giles S, Rücklin M, Donoghue PCJ. 2013. Histology of “placoderm” dermal skeletons:
692 Implications for the nature of the ancestral gnathostome. *Journal of Morphology*
693 274:627-644. DOI: 10.1002/jmor.20119.
- 694 Goloboff PA, Carpenter JM, Arias JS, Rafael D, Esquivel M. 2008. Weighting against
695 homoplasy improves phylogenetic analysis of morphological data sets. *Cladistics*
696 24:758-773.
- 697 Goujet DF, Young GC. 1995. Interrelationships of placoderms revisited. *Geobios*,
698 *Mémoire Spécial* 19:89-95.
- 699 Gross W. 1965. Über die Placodermen-Gattungen *Asterolepis* und *Tiaraspis* aus dem
700 Devon Belgiens und einen fraglichen *Tiaraspis*-rest aus dem Devon Spitzbergens.
701 *Institut royal des Sciences naturelles de Belgique, Bulletin* 41:1-19.
- 702 Hemmings SK. 1978. The Old Red Sandstone antiarchs of Scotland: *Pterichthyodes* and
703 *Microbrachius*. *Monographs of the Palaeontographical Society* 131:1-64.
- 704 Janvier P. 1995. The brachial articulation and pectoral fin in antiarchs (Placodermi).
705 *Bulletin du Muséum national d'Histoire naturelle, Paris* 17:143-161.
- 706 Janvier P. 1996. *Early Vertebrates*. Oxford: Clarendon Press.
- 707 Janvier P, Pan J. 1982. *Hyrceanaspis bliecki* n.g. n.sp., a new primitive euantiarch
708 (Antiarcha, Placodermi) from the Middle Devonian of northeastern Iran, with a

- 709 discussion on antiarch phylogeny. *Neues Jahrbuch für Geologie und Paläontologie,*
710 *Abhandlungen* 164:364-392.
- 711 Jia L-T, Zhu M, Zhao W-J. 2010. A new antiarch fish from the Upper Devonian
712 Zhongning Formation of Ningxia, China. *Palaeoworld* 19:136-145. DOI:
713 10.1016/j.palwor.2010.02.002
- 714 Johanson Z, Young GC. 1999. New *Bothriolepis* (Antiarchi: Placodermi) from the
715 Braidwood region, New South Wales, Australia (Middle-Late Devonian). *Records of*
716 *the Australian Museum supplement* 57:55-75.
- 717 Karatajūte-Talimaa VN. 1963. Genus *Asterolepis* from the Devonian of Russian
718 Platform. In: Grigelis A, and Karatajūte-Talimaa VN, eds. *Voprosy geologii Litvy* [= *Data on Geology of Lithuania*]. Vilnius: Institute of Geology and Geography, 65-
719 224.
- 720
- 721 Karatajūte-Talimaa VN. 1966. Bothriolepids of Šventoji Regional Stage of the Baltics. In:
722 Grigelis A, ed. *Paleontologiya i stratigrafiya Pribaltiki i Belorussii* [= *Palaeontology*
723 *and Stratigraphy of Baltics and Byelorussia*] I (VI). Vilnius: Mintis, 191-279.
- 724 King B, Qiao T, Lee MSY, Zhu M, Long JA. 2016. Bayesian morphological clock
725 methods resurrect placoderm monophyly and reveal rapid early evolution in jawed
726 vertebrates. *Systematic Biology* 66:599-516. DOI: 10.1093/sysbio/syw107.
- 727 Liu S-F. 1983. Biogeography of Silurian and Devonian vertebrates in China. *Vertebrata*
728 *PalAsiatica* 21:292-300.
- 729 Liu T-S, P'an K. 1958. Devonian fishes from Wutung Series near Nanking, China.
730 *Palaeontologica Sinica, new series C* 141:1-41.
- 731 Liu Y-H. 1963. On the Antiarchi from Chutsing, Yunnan. *Vertebrata PalAsiatica* 7:39-46.
- 732 Liu Y-H. 1991. On a new petalichthyid, *Eurycaraspis incilis* gen. et sp. nov., from the
733 Middle Devonian of Zhanyi, Yunnan. In: Chang M-M, Liu Y-H, and Zhang G-R, eds.
734 *Early Vertebrates and Related Problems of Evolutionary Biology*. Beijing: Science
735 Press, 139-177.
- 736 Liu Y-H, Gai Z-K, Zhu M. 2018. New findings of galeaspids (Agnatha) from the Lower
737 Devonian of Qujing, Yunnan, China. *Vertebrata PalAsiatica* 56: 1-15.
- 738 Liu Y-H, Zhu M, Gai Z-K, Lu L-W. 2015. Subclass Galeaspida. In: Zhu M, ed.
739 *Palaeovertebrata Sinica, Volume I, Fishes, Fascicle 1, Agnathans*. Beijing: Science
740 Press, 141-272.
- 741 Liu Y-H, Wang J-Q. 1973. Discussion of several problems regarding the Devonian of
742 eastern Yunnan. *Vertebrata PalAsiatica* 11:17.
- 743 Long JA. 1983. New bothriolepid fish from the late Devonian of Victoria, Australia.
744 *Palaeontology* 26:295-320.
- 745 Long JA, Mark-Kurik E, Johanson Z, Lee MS, Young GC, Zhu M, Ahlberg PE, Newman
746 M, Jones R, Blauwen JD, Choo B, Trinajstić K. 2015. Copulation in antiarch
747 placoderms and the origin of gnathostome internal fertilization. *Nature* 517:196-
748 199. DOI: 10.1038/nature13825.
- 749 Long JA, Werdelin L. 1986. A new Late Devonian bothriolepid (Placodermi, Antiarcha)

- 750 from Victoria, with description of other species from the state. *Alcheringa* 10:355-
751 399.
- 752 Lu J, Giles S, Friedman M, den Blaauwen JL, Zhu M. 2016. The oldest actinopterygian
753 Highlights the cryptic early history of the hyperdiverse ray-finned fishes. *Current*
754 *Biology* 26:1602-1608. DOI: 10.1016/j.cub.2016.04.045.
- 755 Lukševičs E. 2001. Bothriolepid antiarchs (Vertebrata, Placodermi) from the Devonian of
756 the north-western part of the East European Platform. *Geodiversitas* 23:489-609.
- 757 Maddison WP, Maddison DR. 2000. MacClade. Version 4.0 analysis of phylogeny and
758 character evolution. Sunderland, Massachusetts: Sinauer Associates.
- 759 McCoy F. 1848. On some new fossil fish from the Carboniferous Period. *Annals And*
760 *Magazine of Natural History* 2:1-10, 115-133.
- 761 Miles RS. 1968. The Old Red Sandstone antiarchs of Scotland: Family Bothriolepididae.
762 *Palaeontographical Society Monographs* 122:1-130.
- 763 Miles RS. 1971. The Holonematidae (placoderm fishes), a review based on new
764 specimens of *Holonema* from the Upper Devonian of western Australia.
765 *Philosophical Transactions of the Royal Society of London, Series B* 263:101-234.
- 766 Miles RS. 1973. Relationships of acanthodians. In: Greenwood PH, Miles RS, and
767 Patterson C, eds. *Interrelationships of Fishes*. London: Academic Press, 63-103.
- 768 Miles RS. 1977. Dipnoan (lungfish) skulls and the relationships of the group: a study
769 based on new species from the Devonian of Australia. *Zoological Journal of the*
770 *Linnean Society* 61:1-328.
- 771 Moloshnikov SV. 2004. Crested antiarch *Bothriolepis zadonica* H.D. Obrucheva from the
772 lower Famennian of Central European Russia. *Acta Palaeontologica Polonica*
773 49:135-146.
- 774 Moloshnikov SV. 2008. Devonian antiarchs (Pisces, Antiarchi) from central and southern
775 European Russia. *Paleontological Journal* 42:691-773. DOI:
776 10.1134/s0031030108070010.
- 777 Moloshnikov SV. 2010. Middle Devonian bothriolepiform antiarchs (Pisces, Placodermi)
778 from central Kazakhstan and their implication for the antiarch system and
779 phylogeny. *Paleontological Journal* 44:195-208.
- 780 Nielsen E. 1942. Studies on Triassic fishes from East Greenland. I. *Glaucolepis* and
781 *Boreosomus*. *Meddelelser om Grønland* 138:1-403.
- 782 Obruchev DV. 1933. Description of four new fish species from the Devonian of Leningrad
783 Province. *Materials of the Central Scientific Geological and Prospecting Institute,*
784 *Palaeontology and Stratigraphy Magazine* 1:12-14.
- 785 P'an K, Wang S-T, Gao L-D, Hou J-P. 1978. The Devonian System of South China. In:
786 Institute of Geology and Mineral Resources of the Chinese Academy of Geological
787 Sciences, ed. *Symposium on the Devonian System of South China*, Beijing:
788 Geological Press, 240-269.
- 789 Pan J, Dineley DL. 1988. A review of early (Silurian and Devonian) vertebrate
790 biogeography and biostratigraphy of China. *Proceedings of the Royal Society of*

- 791 *London Series B-Biological Sciences* 235:29-61.
- 792 Pan J, Lu L-W. 1997. *Grammaspis*, a new antiarch fish (placoderm) from Early Devonian
793 of Jiangyou, Sichuan Province. In: *Evidence of Evolution-Essays in Honor of Prof*
794 *Chungchien Young on the Hundredth Anniversary of His Birth*. Beijing: China
795 Ocean Press, 97-103.
- 796 Pan Z-H, Zhu M, Zhu Y-A, Jia L-T. 2015. A new petalichthyid placoderm from the Early
797 Devonian of Yunnan, China. *Comptes Rendus Palevol* 14:125-137. DOI:
798 10.1016/j.crpv.2014.10.006
- 799 Pan Z-H, Zhu M, Zhu Y-A, Jia L-T. 2017. A new antiarch placoderm from the Emsian
800 (Early Devonian) of Wuding, Yunnan, China. *Alcheringa* 1-12. DOI:
801 10.1080/03115518.2017.1338357.
- 802 Patterson C. 1975. The braincase of pholidophorid and leptolepid fishes, with a review of
803 the actinopterygian braincase. *Philosophical Transactions of the Royal Society of*
804 *London, Series B* 269:275-579.
- 805 Qiao T, King B, Long JA, Ahlberg PE, Zhu M. 2016. Early gnathostome phylogeny
806 revisited: multiple method consensus. *PLoS One* 11:e0163157. DOI:
807 10.1371/journal.pone.0163157.
- 808 Rücklin M, Long JA, Trinajstić K. 2015. A new selenosteid arthrodire ('Placodermi') from
809 the Late Devonian of Morocco. *Journal of Vertebrate Paleontology* 35:e908896.
810 DOI: 10.1080/02724634.2014.908896.
- 811 Racheboeuf P, Phuong TH, Hung NH, Feist M, Janvier P. 2006. Brachiopods,
812 crustaceans, vertebrates, and charophytes from the Devonian Ly Hoa, Nam Can
813 and Dong Tho Formations of Central Vietnam. *Geodiversitas* 28:5-36.
- 814 Ritchie A, Wang S-T, Young GC, Zhang G-R. 1992. The Sinolepidae, a family of
815 antiarchs (placoderm fishes) from the Devonian of South China and eastern
816 Australia. *Records of the Australian Museum* 44:319-370. DOI: 10.3853/j.0067-
817 1975.44.1992.38.
- 818 Stensiö E. 1969. Elasmobranchiomorphi Placodermata Arthrodires. In: Piveteau J, ed.
819 *Traité de Paléontologie*. Paris: Masson, 71-692.
- 820 Stensiö EA. 1925. On the head of the macropetalichthyids with certain remarks on the
821 head of the other arthrodires. *Geological Series* 4:87-197.
- 822 Stensiö EA. 1931. Upper Devonian vertebrates from East Greenland collected by the
823 Danish Greenland expeditions in 1929 and 1930. *Meddelelser om Grønland* 86:1-
824 212.
- 825 Stensiö EA. 1948. On the Placodermi of the Upper Devonian of East Greenland. II.
826 Antiarchi: subfamily Bothriolepinae. With an attempt at a revision of the previously
827 described species of that family. *Meddelelser om Grønland* 139:1-622.
- 828 Swofford DL. 2003. *PAUP*: Phylogenetic analysis using parsimony (* and other*
829 *methods)*, version 4.0b 10. Sunderland, Massachusetts: Sinauer Associates.
- 830 Tông-Dzuy T, Janvier P. 1990. Les Vertébrés du Dévonien inférieur du Bac Bo oriental
831 (provinces de Bac Thaï et Lang Son, Viêt Nam). *Bulletin du Muséum national*

- 832 *d'Histoire naturelle, Paris 4e sér, Section C* 12:143-223.
- 833 Tông-Dzuy T, Janvier P, Phuong TH. 1996. Fish suggests continental connections
834 between the Indochina and South China blocks in Middle Devonian time. *Geology*
835 24:571-574.
- 836 Wang J-Q. 1991. The Antiarchi from Early Silurian of Hunan. *Vertebrata Palasiatica*
837 29:240-244.
- 838 Wang J-Q, Wang N-Z. 1983. A new genus of Coccoosteidae. *Vertebrata Palasiatica* 21:1-
839 8.
- 840 Wang N-Z. 1984. Thelodont, acanthodian and chondrichthyan fossils from the Lower
841 Devonian of southwest China. *Proceedings of the Linnean Society of New South*
842 *Wales* 107:419-441.
- 843 Wang S-T. 1988. Vertebrate Paleontology. In: Sciences CAoG, ed. *The Devonian*
844 *System and the stratigraphic palaeontology in Longmenshan Mountain Region,*
845 *Sichuan*. Beijing: Geological Publishing House, 339-345.
- 846 Wang W, Qu Q-M, Zhu M. 2010. A brief review of the Middle Palaeozoic vertebrates
847 from Southeast Asia. *Palaeoworld* 19:27-36. DOI: 10.1016/j.palwor.2009.12.005.
- 848 Wang Z-S. 1994. New discovery of yunnanolepids - *Heteroyunnanolepis qujingensis*
849 gen. et sp. nov. *Vertebrata Palasiatica* 32:11.
- 850 Xue J-Z. 2012. Lochkovian plants from the Xitun Formation of Yunnan, China, and their
851 palaeophytogeographical significance. *Geological Magazine* 149:333-344.
- 852 Young GC. 1979. New information on the structure and relationships of *Buchanosteus*
853 (Placodermi: Euarthrodira) from the Early Devonian of New South Wales.
854 *Zoological Journal of the Linnean Society* 66:309-352.
- 855 Young GC. 1981a. Biogeography of Devonian vertebrates. *Alcheringa* 5:225-243.
- 856 Young GC. 1981b. New Early Devonian brachythoracids (placoderm fishes) from the
857 Taemas-Wee Jasper region of New South Wales. *Alcheringa* 5:245-271.
- 858 Young GC. 1983. A new antiarchan fish (Placodermi) from the Late Devonian of
859 southeastern Australia. *BMR Journal of Australian Geology & Geophysics* 8:71-81.
- 860 Young GC. 1984. Reconstruction of the jaws and braincase in the Devonian placoderm
861 fish *Bothriolepis*. *Palaeontology* 27:635-661.
- 862 Young GC. 1988. Antiarchs (placoderm fishes) from the Devonian Aztec Silstone,
863 Southern Victoria Land, Antarctica. *Palaeontographica Abt A* 202:1-125.
- 864 Young GC. 2005. Early Devonian arthrodire remains (Placodermi, ?Holonematidae) from
865 the Burrinjuck area, New South Wales, Australia. *Geodiversitas* 27:201-219.
- 866 Young GC. 2008. The relationships of antiarchs (Devonian placoderm fishes)—Evidence
867 supporting placoderm monophyly. *Journal of Vertebrate Paleontology* 28:626-636.
- 868 Young GC. 2010. Placoderms (armored fish): dominant vertebrates of the Devonian
869 period. *Annual Review of Earth and Planetary Sciences* 38:523-550.
870 10.1146/annurev-earth-040809-152507
- 871 Young GC, Gorter JD. 1981. A new fish fauna of Middle Devonian age from the
872 Taemas/Wee Jasper region of New South Wales. *Bulletin of the Bureau of Mineral*

- 873 *Resources Geology and Geophysics Australia* 209:85-147.
- 874 Young GC, Zhang G-R. 1992. Structure and function of the pectoral joint and operculum
875 in Antiarchs, Devonian placoderm fishes. *Palaeontology* 35:22.
- 876 Young GC, Zhang G-R. 1996. New information on the morphology of yunnanolepid
877 antiarchs (placoderm fishes) from the Early Devonian of South China. *Journal of*
878 *Vertebrate Paleontology* 16:623-641.
- 879 Zhang G-R. 1978. The antiarchs from the Early Devonian of Yunnan. *Vertebrata*
880 *PalAsiatica* 16:147-186.
- 881 Zhang G-R, Wang J-Q, Wang N-Z. 2001. The structure of pectoral fin and tail of
882 Yunnanolepidoidei, with a discussion of the pectoral fin of chuchinolepids.
883 *Vertebrata PalAsiatica* 39:9-19.
- 884 Zhang G-R, Young GC. 1992. A new antiarch (placoderm fish) from the Early Devonian
885 of South China. *Alcheringa* 16:219-240.
- 886 Zhang M-M. 1980. Preliminary note on a Lower Devonian antiarch from Yunnan, China.
887 *Vertebrata PalAsiatica* 18:179-190.
- 888 Zhao W-J, Wang N-Z, Zhu M, Mann U, Herten U, Lucke A. 2011. Geochemical
889 stratigraphy and microvertebrate assemblage sequences across the
890 Silurian/Devonian transition in South China. *Acta Geologica Sinica (English*
891 *Edition)* 85:340-353.
- 892 Zhao W-J, Zhu M, Liu S, Pan Z-H, L-T. 2016. A new look at the Silurian fish-bearing
893 strata around the Shanmen Reservoir in Lixian, Hunan province. *Journal of*
894 *Stratigraphy* 40:341-350.
- 895 Zhu M. 1996. The phylogeny of the Antiarcha (Placodermi, Pisces), with the description
896 of Early Devonian antiarchs from Qujing, Yunnan, China. *Bulletin du Muséum*
897 *national d'Histoire naturelle* 18:233-347.
- 898 Zhu M. 2014. Bone gain and loss: insights from genomes and fossils. *National Science*
899 *Review* 1:490-497.
- 900 Zhu M, Ahlberg PE, Pan Z-H, Zhu Y-A, Qiao T, Zhao W-J, Jia L-T, Lu J. 2016. A Silurian
901 maxillate placoderm illuminates jaw evolution. *Science* 354:334-336. DOI:
902 10.1126/science.aah3764.
- 903 Zhu M, Janvier P. 1996. A small antiarch, *Minicrania lirouyii* gen. et sp. nov., from the
904 Early Devonian of Qujing, Yunnan (China), with remarks on antiarch phylogeny.
905 *Journal of Vertebrate Paleontology* 16:1-15.
- 906 Zhu M, Wang J-Q, Fan J-H. 1994. Early Devonian fishes from Guijiatun and Xujiachong
907 Formations of Qujing, Yunnan, and related biostratigraphic problems. *Vertebrata*
908 *PalAsiatica* 32:1-20.
- 909 Zhu M, Yu X-B. 2002. A primitive fish close to the common ancestor of tetrapods and
910 lungfish. *Nature* 418:767-770.
- 911 Zhu M, Yu X-B, Ahlberg PE. 2001. A primitive sarcopterygian fish with an eyestalk.
912 *Nature* 410:81-84.
- 913 Zhu M, Yu X-B, Janvier P. 1999. A primitive fossil fish sheds light on the origin of bony

- 914 fishes. *Nature* 397:607-610.
- 915 Zhu M, Yu X-B, Wang W, Zhao W-J, Jia L-T. 2006. A primitive fish provides key
916 characters bearing on deep osteichthyan phylogeny. *Nature* 441:77-80.
- 917 Zhu M, Yu X-B, Ahlberg PE, Choo B, Lu J, Qiao T, Qu Q-M, Zhao W-J, Jia L-T, Blom H,
918 Zhu Y-A. 2013. A Silurian placoderm with osteichthyan-like marginal jaw bones.
919 *Nature* 502:188-193. DOI: 10.1038/nature12617.
- 920 Zhu M, Yu X-B, Choo B, Wang J-Q, Jia L-T. 2012. An antiarch placoderm shows that
921 pelvic girdles arose at the root of jawed vertebrates. *Biology Letters* 8:453-456.
922 DOI: 10.1098/rsbl.2011.1033.
- 923 Zhu Y-A, Zhu M, Wang J-Q. 2016. Redescription of *Yinostius major* (Arthrodira:
924 Heterostiidae) from the Lower Devonian of China, and the interrelationships of
925 Brachythoraci. *Zoological Journal of the Linnean Society* 176:806-834. DOI:
926 10.1111/zoj.12356.

Figure 1

Holotype and paratype of *Phymolepis cuifengshanensis*.

(A-C) IVPP V4425.3, holotype, trunk shield in dorsal (A), ventral (B) and right lateral (C) views. (D-E) IVPP V4425.6, paratype, PMD in dorsal (D) and ventral (E) views. Abbreviations: aa, anterior angle of PMD; ADL, anterior dorsolateral plate; ala, anterolateral angle of PMD; AMD, anterior median dorsal plate; AVL, anterior ventrolateral plate; cf.AMD, area overlapping AMD; cf.PDL, area overlapping PDL; cr.tp, *crista transversalis interna posterior*; ddr, dorsal diagonal ridge of trunk shield; dl, dorsolateral ridge of trunk shield; dmr, dorsal median ridge; la, lateral angle of PMD; lc, main lateral line canal; lr, lateral ridge of lateral wall of trunk shield; MV, median ventral plate; pa, posterior angle of PMD; pda, posterior dorsal angle; PDL, posterior dorsolateral plate; pf, pectoral fossa; PL, posterior lateral plate; pla, posterolateral angle of PMD; plal, posterolateral angle of AMD; plr, posterior lateral ridge of PMD; PMD, posterior median dorsal plate; pr.p, posterior process of PMD; pt2, posterior ventral pit of dorsal wall of trunk shield; PVL, posterior ventrolateral plate; r.C, ridge caused by Chang's apparatus; vl, ventrolateral ridge of trunk shield. Red arrow represents the direction of the specimen: a, anterior direction. Scale bar equals 1 cm.

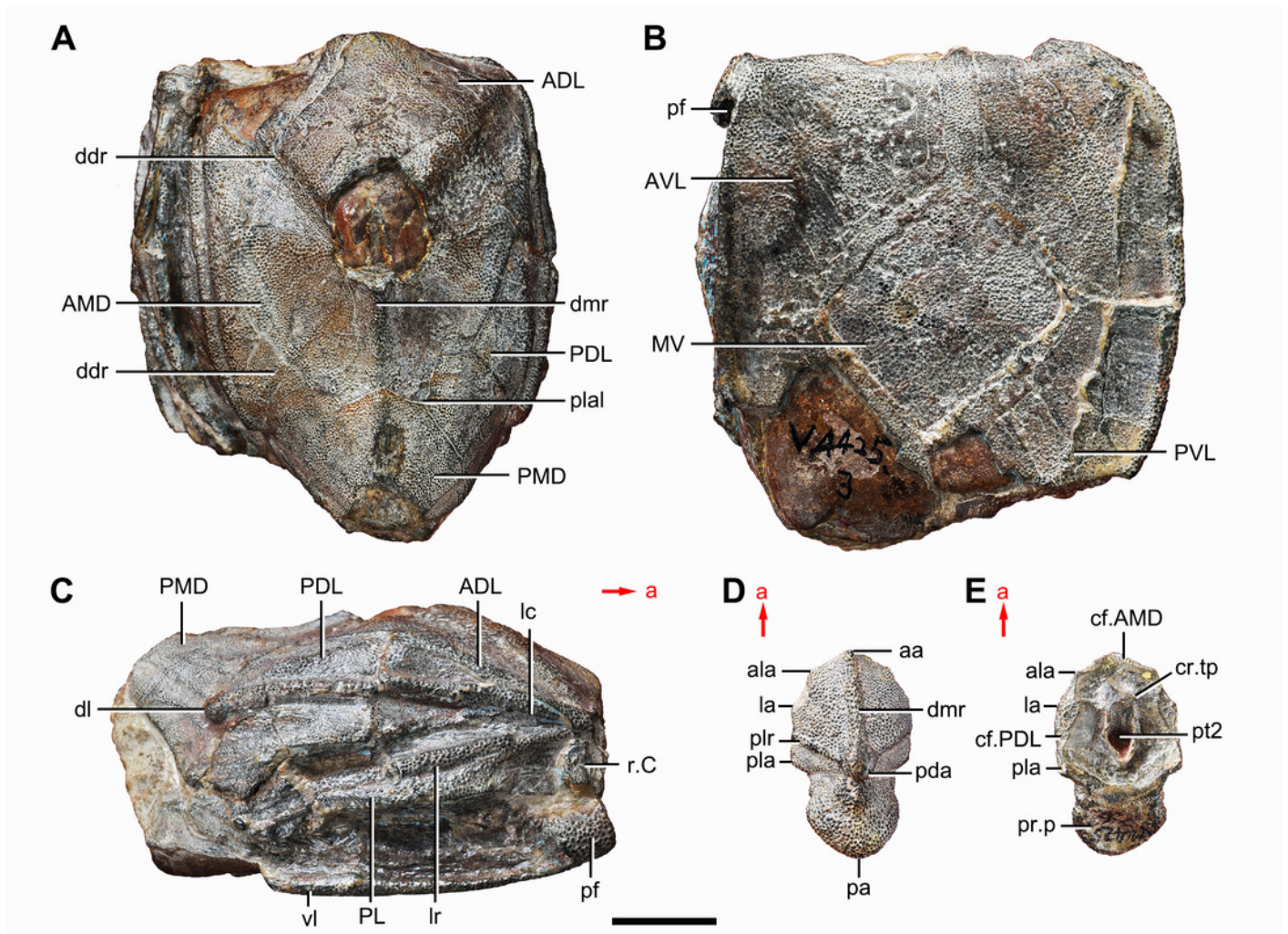


Figure 2

Paratype of *Phymolepis cuifengshanensis* (IVPP V4425.1).

(A) Dorsal view. (B) Ventral view. (C) Right lateral view. (D-E) Anterior view, photo (D) and drawing (E). Abbreviations: ADL, anterior dorsolateral plate; AMD, anterior median dorsal plate; AVL, anterior ventrolateral plate; cit, *crista transversalis interna anterior*; ddr, dorsal diagonal ridge of trunk shield; dma, tergal angle of trunk shield; dmr, dorsal median ridge of trunk shield; f.ca, fossa for neck-joint; iar, infra-articular ridge; lc, main lateral line canal; MV, median ventral plate; o.C, opening of Chang's apparatus; pbl, postbranchial lamina; PDL, posterior dorsolateral plate; PL, posterior lateral plate; pnoa, postnuchal ornamented corner of ADL; PVL, posterior ventrolateral plate; r.C, ridge caused by Chang's apparatus; sar, supra-articular ridge. Red arrow represents the direction of the specimen: a, anterior direction. Scale bars equal 1 cm.

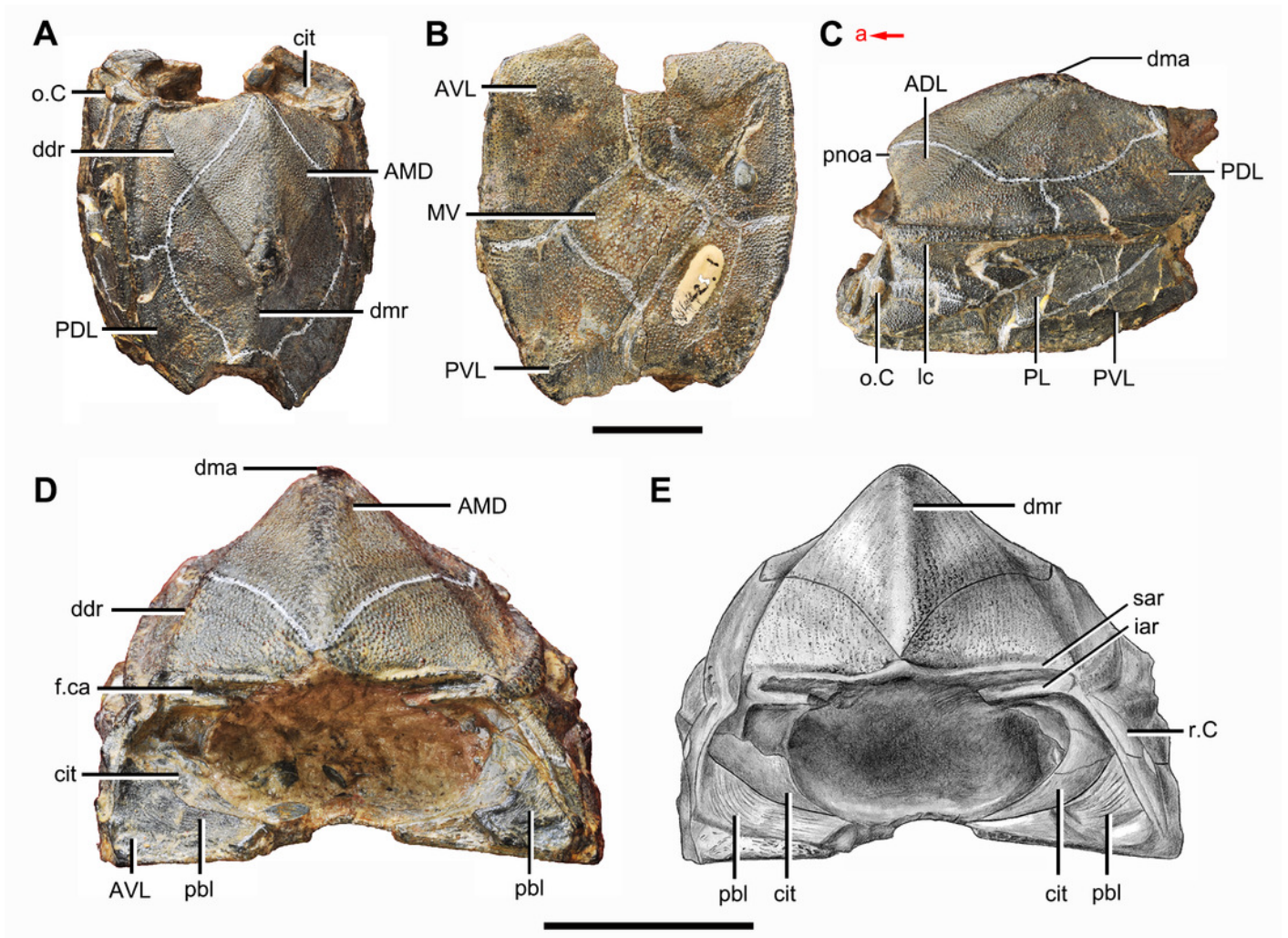


Figure 3

Paratype of *Phymolepis cuifengshanensis* (IVPP V4425.2).

(A) Dorsal view. (B) Ventral view. (C) Right lateral view. (D) Anterior view. Abbreviations: ADL, anterior dorsolateral plate; AMD, anterior median dorsal plate; AVL, anterior ventrolateral plate; ddr, dorsal diagonal ridge of trunk shield; dl, dorsolateral ridge of trunk shield; dma, tergal angle; dmr, dorsal median ridge; dtr, dorsal transverse ridge of trunk shield; La, lateral plate; lr, lateral ridge of lateral wall of trunk shield; MV, median ventral plate; Nu, nuchal plate; or, oblique ridge of lateral wall of trunk shield; orb, orbital fenestra; PDL, posterior dorsolateral plate; PL, posterior lateral plate; PM, postmarginal plate; pmc, postmarginal sensory canal; pnoa, postnuchal ornamented corner of ADL; PNu, paranuchal plate; PP, postpineal plate; PVL, posterior ventrolateral plate; SL, semilunar plate; vl, ventrolateral ridge of trunk shield. Scale bar equals 1 cm.

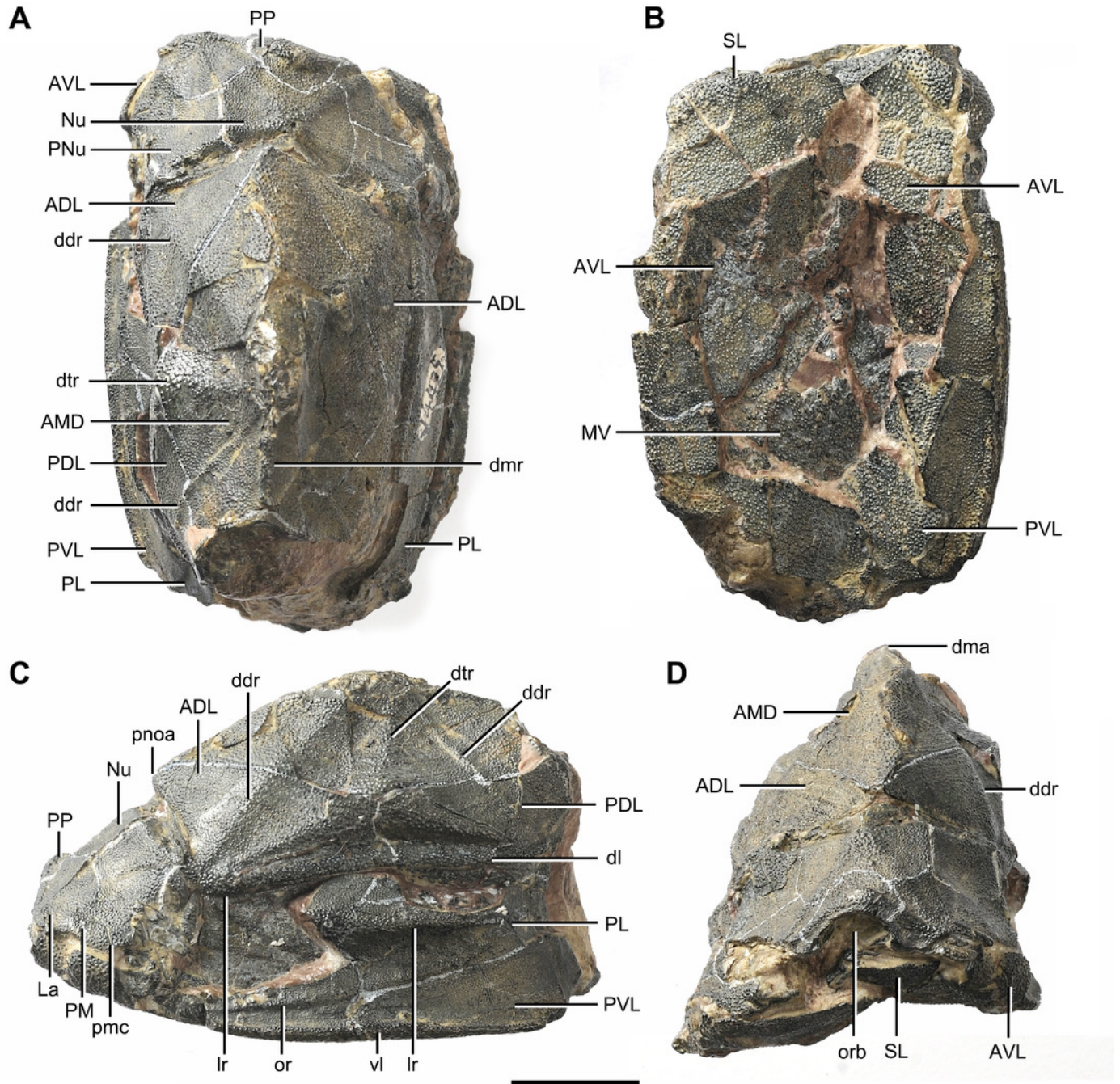


Figure 4

Yunnanolepis parvus (IVPP V4425.7).

(A) Dorsal view. (B) Ventral view. (C) Anterior view. (D) Right lateral view. (E) Left lateral view. Abbreviations: ADL, anterior dorsolateral plate; AMD, anterior median dorsal plate; AVL, anterior ventrolateral plate; cit, *crista transversalis interna anterior*; dma, tergal angle; dmr, dorsal median ridge; pbl, postbranchial lamina; PDL, posterior dorsolateral plate; PL, posterior lateral plate; PMD, posterior median dorsal plate; p.pf, plates of pectoral fin; PVL, posterior ventrolateral plate. Red arrow represents the direction of the specimen: a, anterior direction; p, posterior direction. Scale bar equals 5 mm.

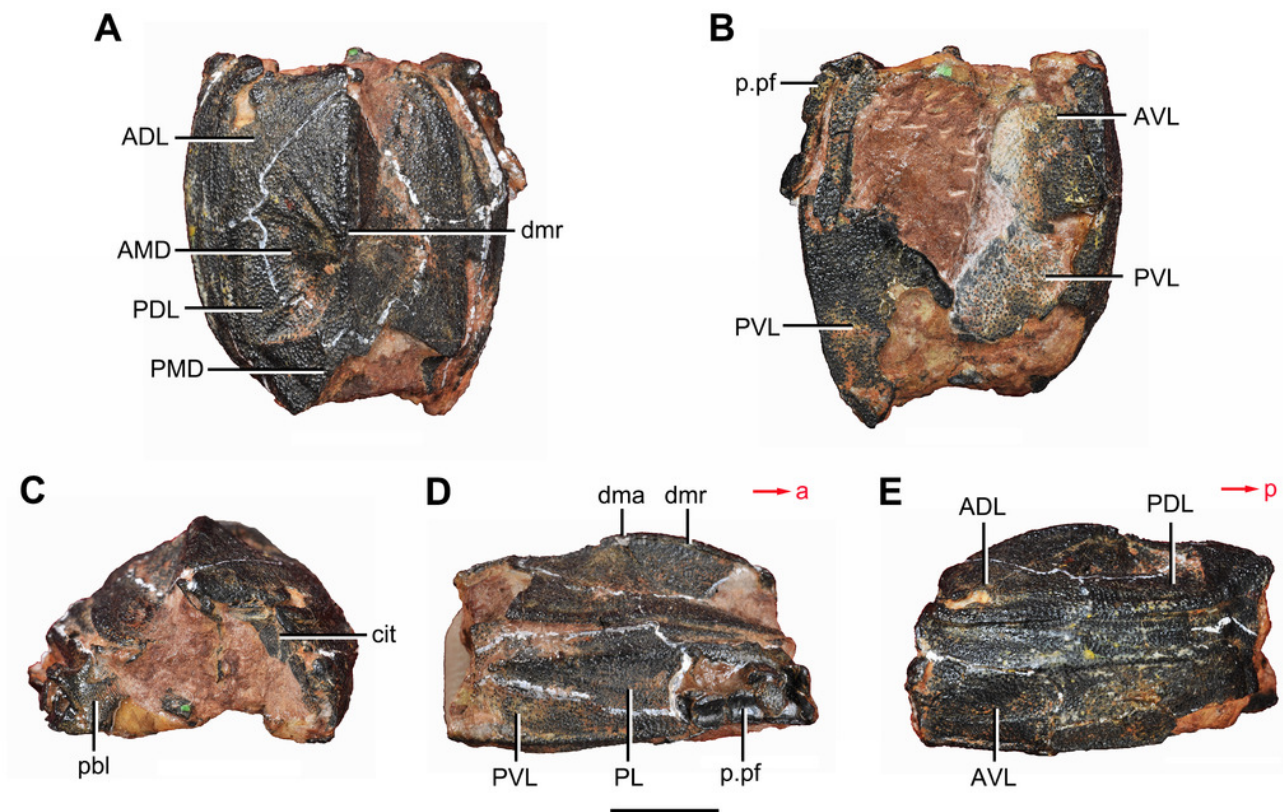


Figure 5

Outline restoration of the dermal shield of *Phymolepis cuifengshanensis*.

(A) Dorsal view. (B) Ventral view. (C) Right lateral view. Stripped lines delineate the unknown part. Scale bar equals 5 mm.

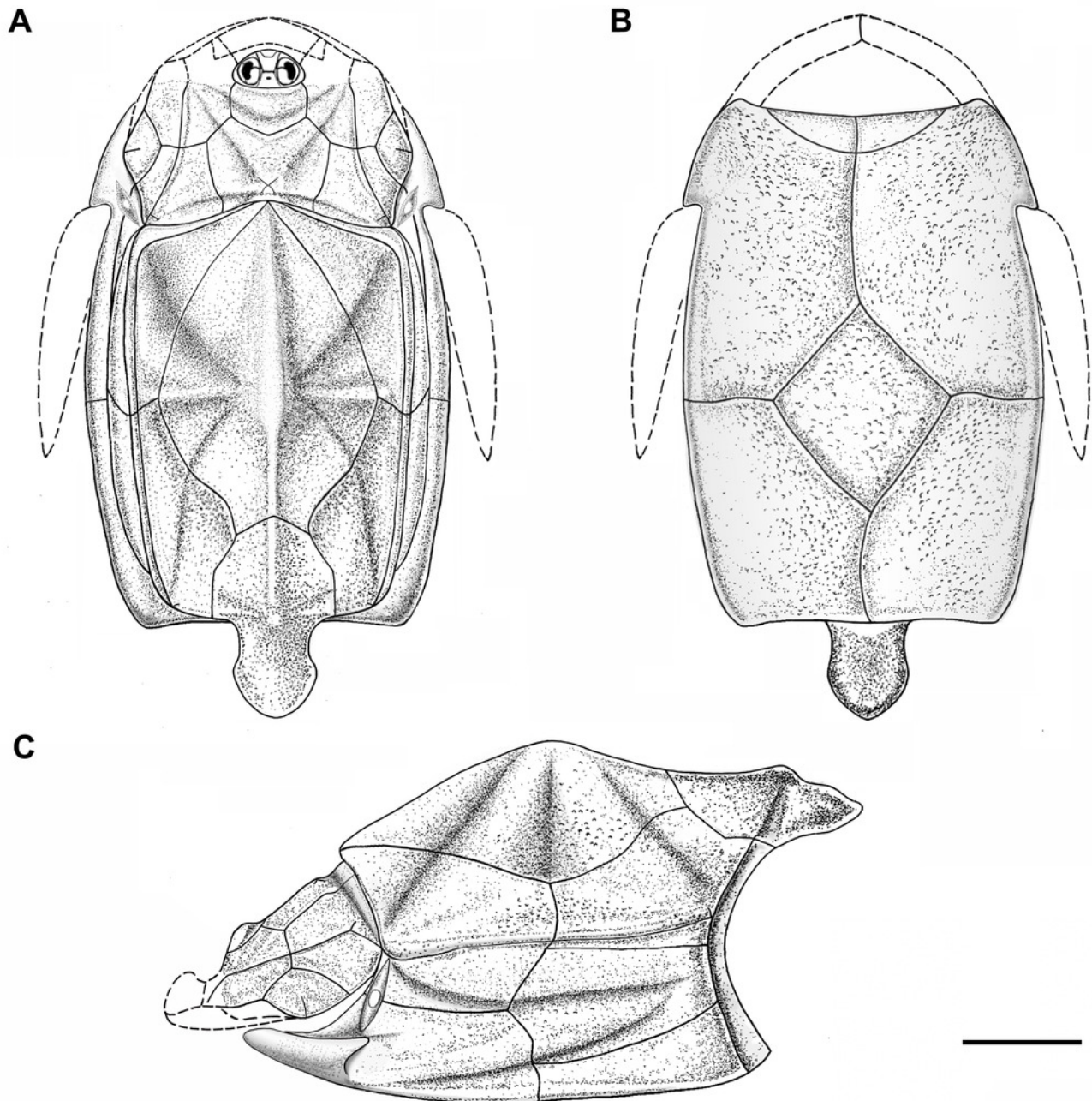


Figure 6

Life reconstruction of *Phymolepis cuifengshanensis*.

Artwork by Dinghua Yang.



Figure 7

Head shield of *Phymolepis cuifengshanensis* (IVPP V4425.2) based on high-resolution CT.

(A–B) Three-dimensional reconstructions in dorsal (A) and ventral (B) views. (C–D) Interpretative drawings in dorsal (C) and ventral (D) views. Abbreviations: a₁, a₂, attachment areas for the dermal operculum on the lateral and paranuchal plates, respectively; alr, anterior lateral ridge on head shield; c.csp, cavity for cranio-spinal process; cr.pm, paramarginal crista; cr.po, postorbital crista; cr.tv, transverse nuchal crista; d.end, opening for endolymphatic duct; d.sac, depression for sacculus; dsc, depression caused by semicircular canal; ifc, infraorbital sensory canal; La, lateral plate; lc, main lateral line canal; mpl, middle pit-line; mr, median ridge of postpineal plate; nm, obstructed nuchal margin; Nu, nuchal plate; occ, occipital cross commissure; oem, median occipital eminence; om, obstantic margin of head shield; ood, otico-occipital depression of head shield; orb, orbital fenestra; p.apo, anterior postorbital process; PM, postmarginal plate; pmc, postmarginal sensory canal ; PNu, paranuchal plate; PP, postpineal plate; plc, posterolateral corner of head shield; ppl, posterior pit-line; pp.th, postpineal thickening; ptoc, postobstantic corner of paranuchal plate; sop, supraoccipital pit of head shield; sorb, suborbital fenestra. Scale bar equals 5 mm.

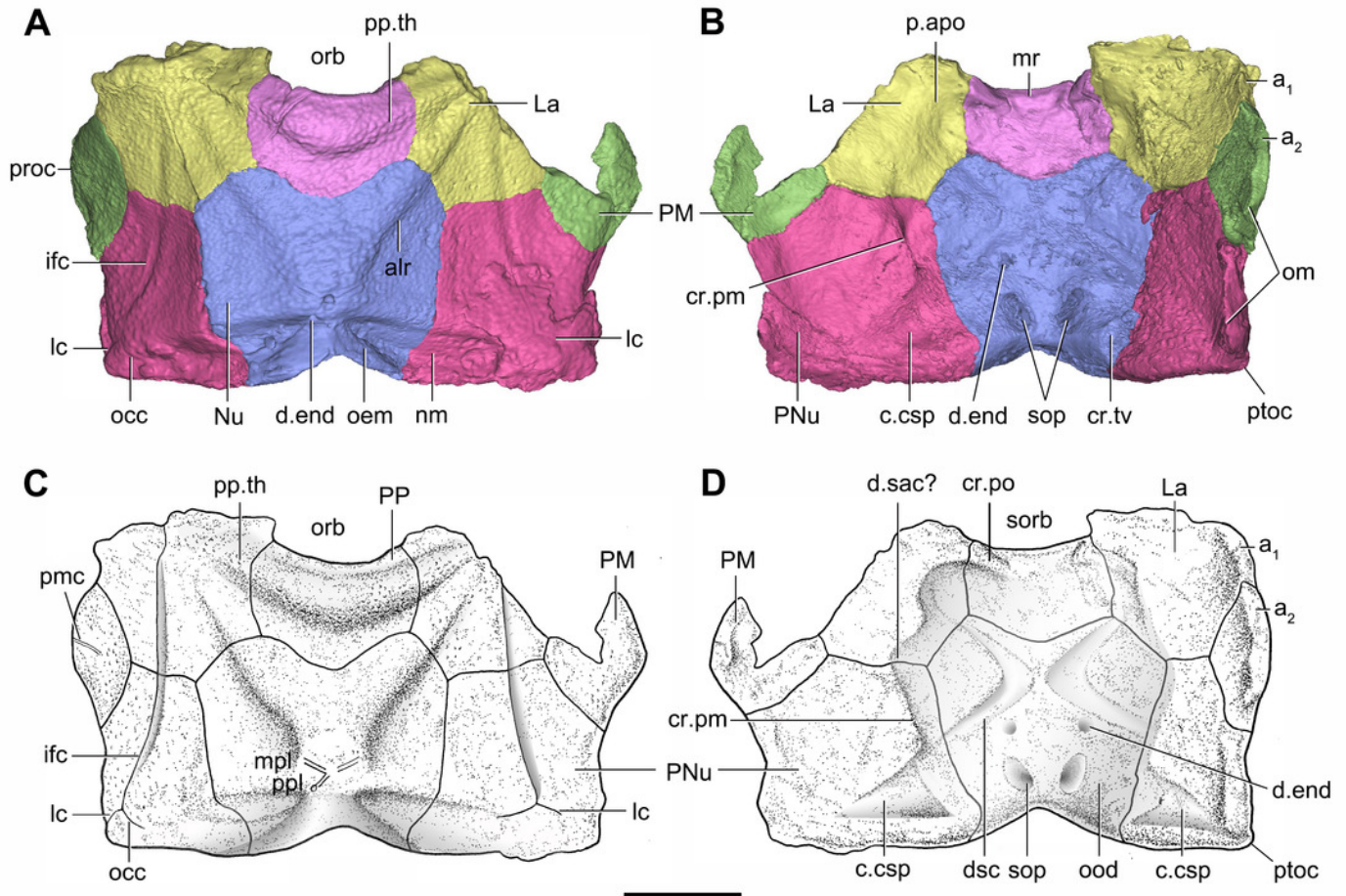


Figure 8

Cavities within the head shield of *Phymolepis cuifengshanensis* (IVPP V4425.2) based on high-resolution CT.

(A) Semi-transparent Nu in dorsal view. (B) Transparent Nu in anterior view. (C) Semi-transparent Nu in lateral view. (D-E) Semi-transparent right PNu in ventral (D) and posterior (E) views. (F) Right PNu in left lateral view. Abbreviations: cr.pm, paramarginal crista; cr.tv, transverse nuchal crista; c.vg, cavity for vagal process, d.end, opening for endolymphatic duct; Nu, nuchal plate; PNu, paranuchal plate. Red arrow represents the direction of the specimen; a, anterior direction; d, dorsal direction; l, left direction; v, ventral direction. Scale bar equals 2 mm.

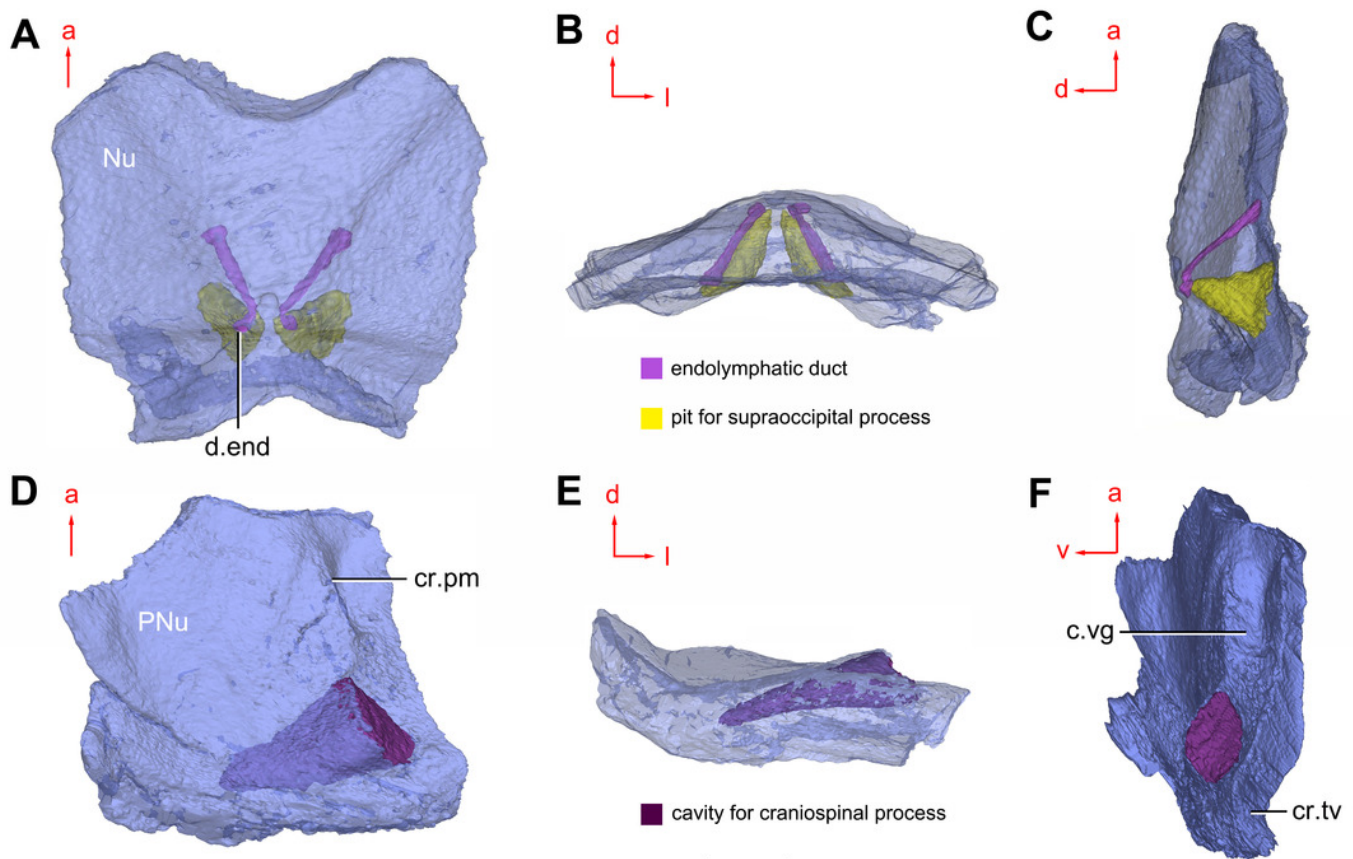


Figure 9

Phymolepis cuifengshanensis (IVPP V4425.2) based on high-resolution CT.

(A-C) Trunk shield in dorsal (A), ventral (B) and anterior (C) views. (D) Head and trunk shields in right lateral view. (E-F) AVL plates and their displaced fragments as preserved (E) and restored (F). Yellow dash lines in (B) delimit restored portions. Abbreviations: ADL: anterior dorsolateral plate; AMD, anterior median dorsal plate; AVL, anterior ventrolateral plate; c.C; cavity of Chang's apparatus; cg, caudal groove of trunk shield; cit, *crista transversalis interna anterior*; cr.tp, *crista transversalis interna posterior*; ddr, dorsal diagonal ridge of trunk shield; dma, tergal angle of trunk shield; dmr, dorsal median ridge of trunk shield; dtr, dorsal transverse ridge of trunk shield; f.ca, fossa for neck-joint; lc, main lateral line canal; lr, lateral ridge of lateral wall of trunk shield; MV, median ventral plate; Nu, nuchal plate; or, oblique ridge of lateral wall of trunk shield; PDL, posterior dorsolateral plate; PL, posterior lateral plate; PM, postmarginal plate; pnoa, postnuchal ornamented corner of ADL; PP, postpineal plate; PVL, posterior ventrolateral plate; pbl, postbranchial lamina; rc, rostrocaudal canal; r.C, ridge caused by Chang's apparatus; SL, semilunar plate. Red arrow represents the direction of the specimen: a, anterior direction; r, right direction. Scale bar equals to 5 mm.

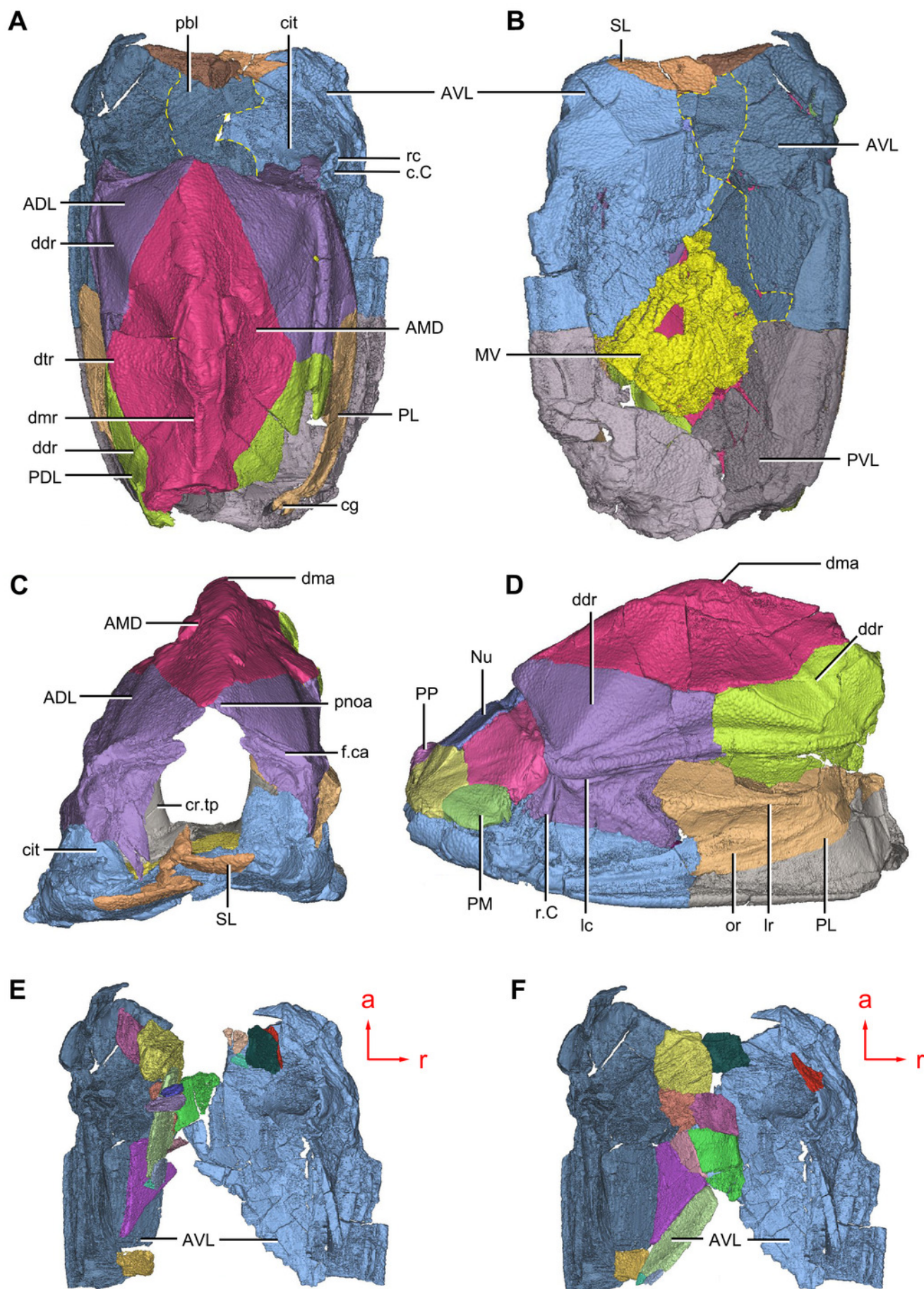


Figure 10

Phymolepis cuifengshanensis (IVPP V4425.2) based on high-resolution CT.

(A) Head shield and anterior portion of trunk shield. (B) Axial section through the left AVL in CT slice, showing the positions of the internal cavity of Chang's apparatus and the rostrocaudal canal. (C) Semi-transparent left ADL in ventral view. (D-E) Semi-transparent right AVL in dorsal (D) and lateral (E) views. (F) Semi-transparent left AVL in dorsal view. Abbreviations: ADL, anterior dorsolateral plate; AVL, anterior ventrolateral plate; c.C; cavity of Chang's apparatus; cit, *crista transversalis interna anterior*; ifc, infraorbital sensory canal; lc, main lateral line canal; pbl, postbranchial lamina; rc, rostrocaudal canal. Red arrow represents the direction of the specimen: a, anterior direction; l, left direction; r, right direction. Scale bar equals 3mm.

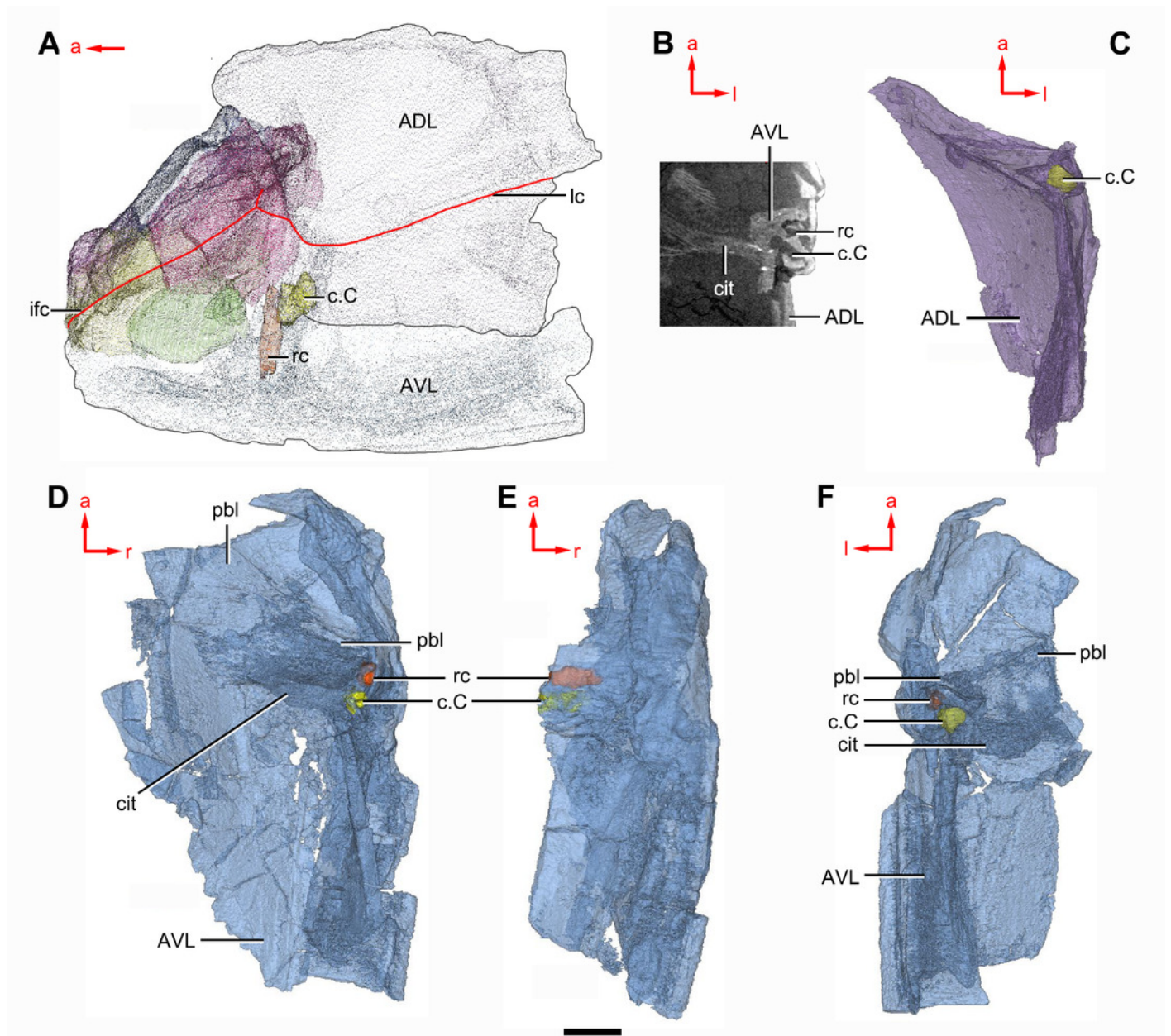


Figure 11

Phymolepis cuifengshanensis (IVPP V4425.2) based on high-resolution CT.

(A) AMD in ventral view. (B) Transverse section through the lateroventral fossa in CT slice. (C) Lateroventral fossa in lateral view. (D) Transverse section through the left caudal groove in CT slice. (E) Axial section through the right caudal groove in CT slice. (F) Left caudal groove in lateral view. Abbreviations: AMD, anterior median dorsal plate; AVL, anterior ventrolateral plate; cf.ADL, area overlapping ADL; cf.PDL, area overlapping PDL; cg, caudal groove of trunk shield; cr.tp, *crista transversalis interna posterior*; f.lv, lateroventral fossa of trunk shield; laI, lateral angle of AMD; ms, median septum; PDL, posterior dorsolateral plate; PL, posterior lateral plate; plal, posterolateral angle of AMD; prv1, anterior ventral process of dorsal wall of trunk shield; pt1, anterior ventral pit of dorsal wall of trunk shield; PVL, posterior ventrolateral plate; wa, outer wall of caudal groove. Red arrow represents the direction of the specimen: a, anterior direction; d, dorsal direction; r, right direction. Scale bars equal 3 mm.

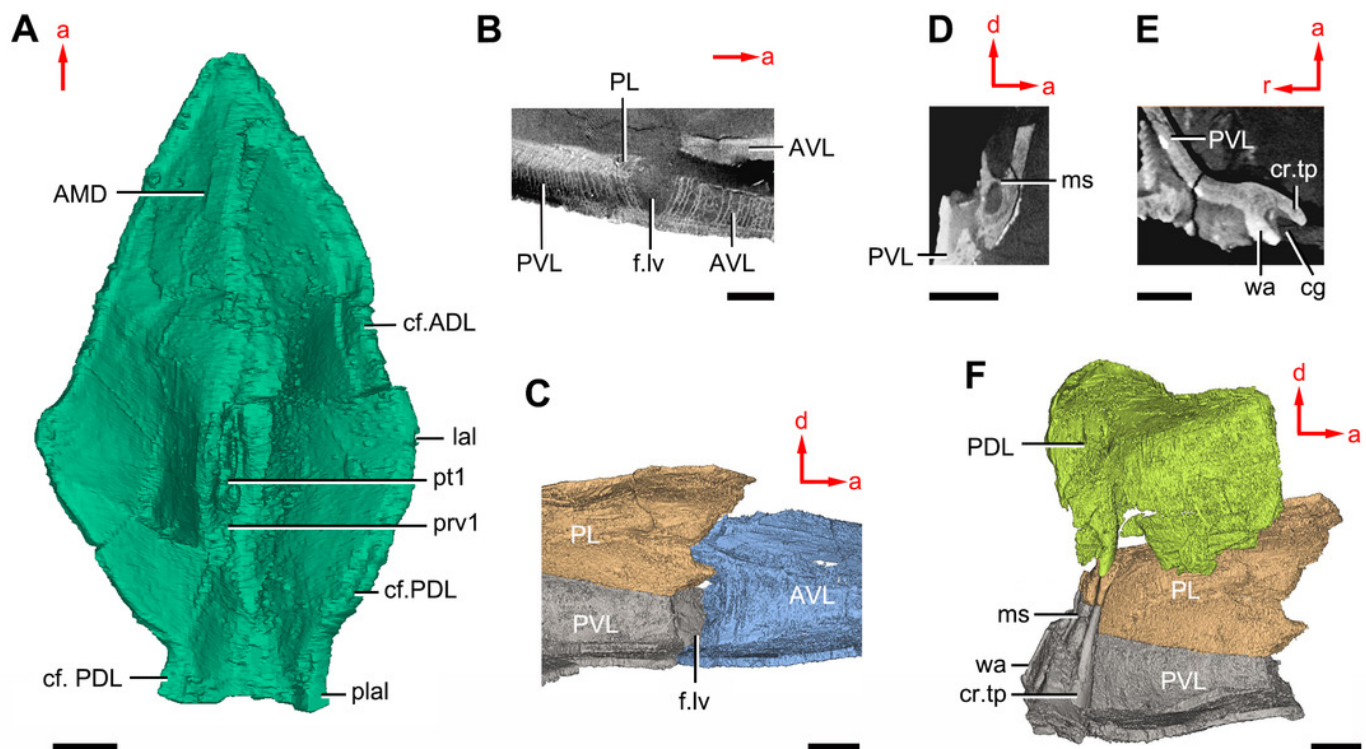


Figure 12

Head shields of *Yunnanolepis chii* in visceral view.

(A) IVPP V2690.1. (B) IVPP V4423.3. Abbreviations: c.csp, cavity for cranio-spinal process; cr.pm, paramarginal crista; cr.po, postorbital crista; cr.tv, transverse nuchal crista; d.end, opening for endolymphatic duct; d.sac, depression for sacculus; dsc, depression caused by semicircular canal; fm, unpaired insertion fossa on head shield for levator muscles; mr, medial ridge of postpineal plate; ood, otico-occipital depression of head shield; p.apo, anterior postorbital process; r.spr, subpremedian ridge; sop, supraoccipital pit of head shield; tlg, transverse lateral groove of head shield. Scale bars equal to 5 mm.

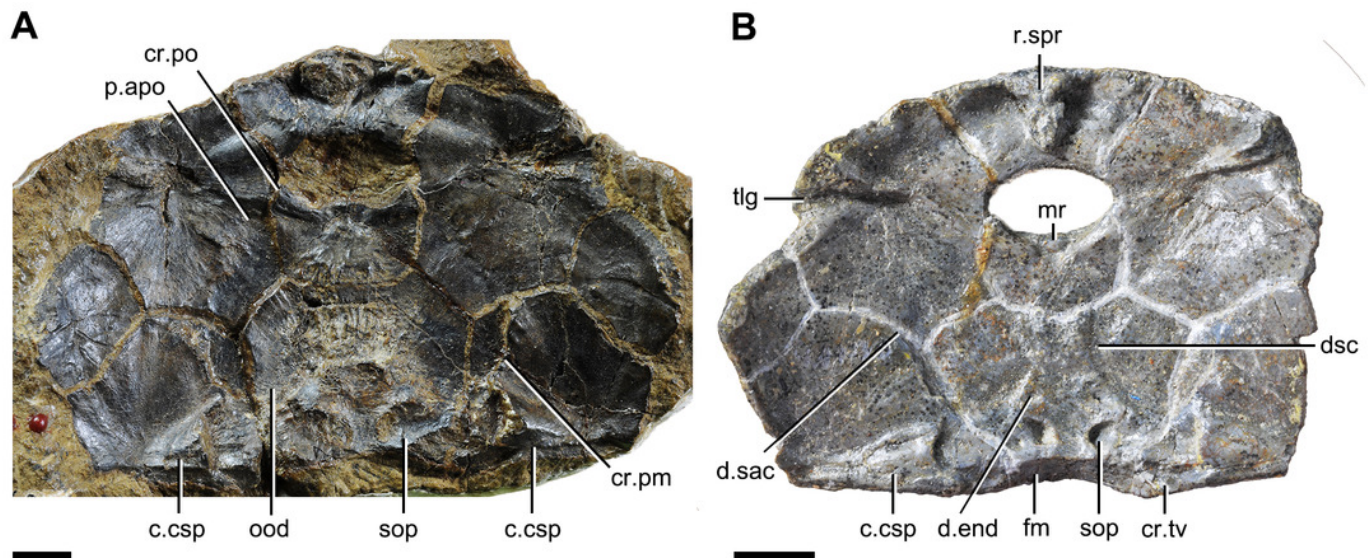


Figure 13(on next page)

Phylogenetic results of antiarchs based on a revised data matrix.

(A) Strict consensus tree of 726 parsimonious trees (tree length = 179; consistency index = 0.4693, homoplasy index = 0.5307, retention index = 0.8045, rescaled consistency index = 0.3775). Numbers above and below nodes represent bootstrap values ($\geq 50\%$ are shown) and Bremer decay indices, respectively. (B) 50 % majority-rule consensus tree of 726 parsimonious trees based on the same dataset as in (A). Numbers next to nodes indicate the percentage of the shortest trees in which the partition is supported (100% are not shown).

Figure 14(on next page)

Phylogenetic results of antiarchs and visceral surface conditions of head shield among major antiarch subgroups.

(A) One of the most parsimonious trees with node numbers defining various clades. Named nodes: 1, Antiarcha; 2, Yunnanolepidoidei; 11, Sinolepididae; 15, Euanarcha; 16, Microbrachiidae; 26, Asterolepidoidei. (B) Restorations of the head shields in ventral view to show endocranial character transformations, redrawn from Ritchie et al. (1992), Young (1983), Stensiö (1948) and (1969). Vertical bars on the right side show the longitudinal proportion of otico-occipital region of endocranium on the head shield (blue region), the location of the confluence of semicircular canals (orange circle), the location of the internal pore for endolymphatic duct (purple circle). Abbreviations: c.csp, cavity for cranio-spinal process; cr.im, inframarginal crista; cr.tv, transverse nuchal crista; cro, median occipital crista of head shield; d.end, opening for endolymphatic duct; dsc, depression caused by semicircular canal; f.cu, cucullaris fossa; fm, unpaired insertion fossa on head shield for levator muscles; p.apo, anterior postorbital process; prnm, posterior process of head shield; sop, supraoccipital pit of head shield; sot, supraotic thickening of head shield; tlg, transverse lateral groove of head shield.

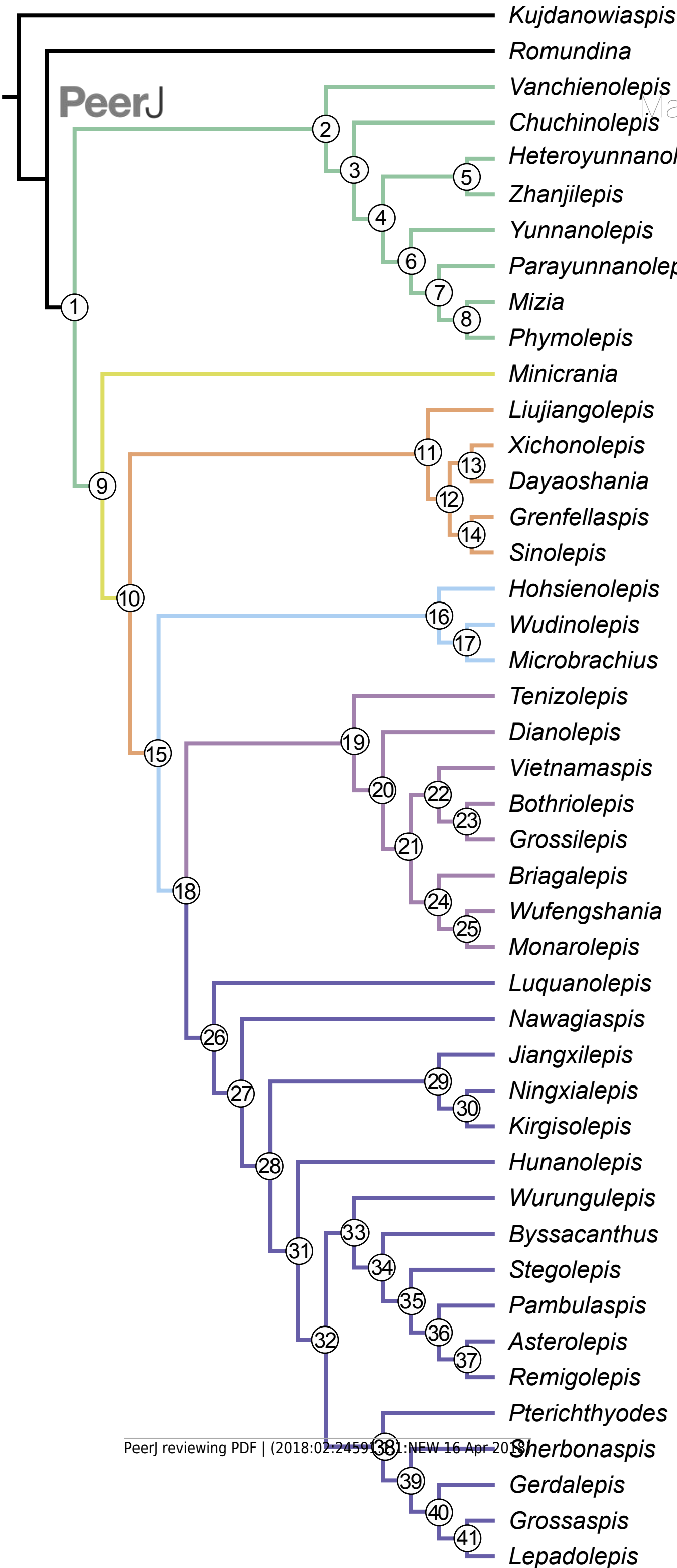
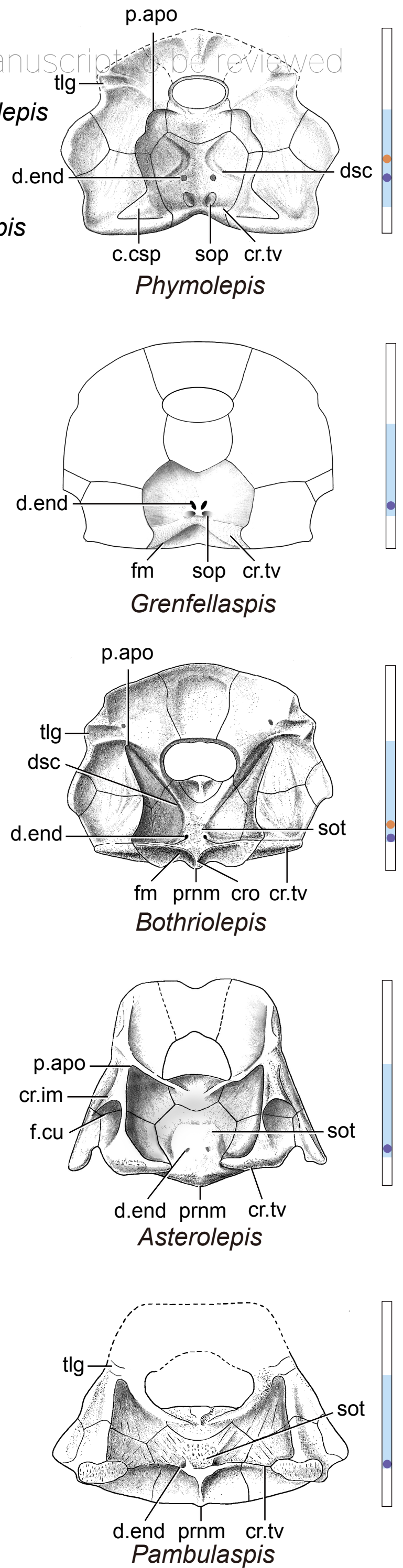
A**B**

Table 1 (on next page)

Measurements (in mm) and ratios for the head shield of *Phymolepis cuihengshanensis* (IVPP V4425.2). Measurements were obtained by means of the digital visualization.

	breadth	length	breadth/length
Postpineal plate	6.72	2.49	2.67
Nuchal plate	10.81	9.67	1.12
Paranuchal plate	8.56	9.13	0.94
Postmarginal plate	4.94	6.39	0.78
Head shield (across preobstantic corners)	24.05		
Orbital fenestra	5.78		
Anterolateral margin of nuchal		3.23	
Posterolateral margin of nuchal		7.91	
Obtected nuchal area		2.65	
Breadth ratio between orbital fenestra and head shield			0.24
Length ratio between posterolateral and anterolateral margins of nuchal			2.45
Length ratio between obtected nuchal area and nuchal			0.27

1

Table 2 (on next page)

Measurements (in mm) and ratios for the trunk shield of *Phymolepis cuihengshanensis*.

Specimen Number		V4425.1	V4425.2	V4425.3
Dorsal wall of trunk shield (excluding posterior median dorsal plate)	Breadth (B)	23.0	22.0	39.0
	Length (L)	31.0	34.0	50.0
	B/L	0.7	0.7	0.8
Lateral wall of trunk shield	Length	30.0	34.0	40.0
	Height (H)	10.0	15.0	20.0
	L/H	3.0	2.3	2.0
Ventral wall of trunk shield	Breadth	28.0	30	45.0
	Length	34.0	48.0	-
	B/L	0.8	0.6	-
Anterior median dorsal plate	Breadth	18.0	22.0	28.0
	Length	26.0	32.0	41.0
	B/L	0.7	0.7	0.7
Anterior dorsolateral plate	Breadth	13.0	14.0	17.0
	Length	17.0	20.0	26.0
	Height	6.0	8.0	11.0
	B/L	0.8	0.7	0.7
	L/H	2.8	2.5	2.4
Anterior ventrolateral plate	Breadth	15.0	20.0	-
	Length	19.5	29.0	-
	B/L	0.8	0.7	-
Posterior dorsolateral plate	Breadth	8.0	9.5	13.0
	Length	15.5	17.0	28.0
	Height	-	4.0	8.0
	B/L	0.5	0.6	0.5
	L/H	-	4.3	3.5
Posterior lateral plate	Length	17.0	19.0	25.0
	Height	7.0	8.0	10.0
	L/H	2.4	2.4	2.5
Posterior ventrolateral plate	Breadth	18.0	20.0	-
	Length	16.0	18.0	-
	Height	7.0	8.0	-
	B/L	1.1	1.1	-
	L/H	2.3	2.3	-
Semilunar plate	Breadth	-	8.0	-
	Length	-	4.0	-
	B/L	-	2.0	-
Median ventral plate	Breadth	13.0	-	23.0
	Length	14.0	-	24.0
	B/L	0.9	-	1.0

